CHEMICAL REVIEWS

REVIEW

pubs.acs.org/CR

Conventional and Unconventional Metal−Organic Frameworks Based on Phosphonate Ligands: MOFs and UMOFs

Kevin J. Gagnon, Houston P. Perry, and Abraham Clearfield*

Texas A&M University, Chemistry Department, Corner of Spence and Ross, College Station, Texas 77843, United States

CONTENTS

1. INTRODUCTION

The class of materials known as metal−organic frameworks, or MOFs, is the subject of an enormous amount of current research. The other reviews in this issue serve as testament to this fact. The defining character of these compounds is their porosity, which can be tuned by changing the geometry and size of the carboxylic acid ligands. In the early years of this research, carboxylate-based MOFs were designed to have ever-greater surface areas, resulting in the astonishing increase from 600 to >5000 m^2/g.[1−6] In addition, interest was keyed toward very large uptake of certain gases such as hydrogen, methane, and carbon dioxide and the possibility of a range of potential gas separations. The number of reported MOFs has skyrocketed as researchers have explored the vast number of possible combinations of ligand design, transition metals, coligands, and structure-directing agents. Many investigators were fascinated by the idea that one could use a set of principles to define structures that would be porous. However, although many papers claim to have created porous products, the structural data is insufficient. One must have a sorption isotherm to prove the extent of porosity.

Carboxylate-based MOFs have been shown to have remarkably high surface area and uniform pore size distribution, but their lack of stability in air and water poses a significant problem if they are to be used in industrial or commercial applications. Divalent metal carboxylates are subject to hydrolysis and usually quite soluble in acid solution. It should be pointed out that other types of MOFs, such as those based on pyrazolate ligands, can be much more robust.[7] Phosphonates form stronger bonds than carboxylates do with metal atoms, so it is natural that investigators should try to prepare phosphonate-based MOFs. From our own experience, monovalent metal phosphonates are highly soluble, even though they may crystallize as supramolecular structures. As the valence of the metal increases, the solubility decreases. Divalent metal phosphonates are soluble enough that single crystals can be obtained by hydrothermal or solvothermal techniques, whereas trivalent and tetravalent metal phosphonates are rarely crystalline as they are highly insoluble and tend to precipitate as poorly ordered layered materials. The tetravalent metal phosphonates are insoluble even in strong acid solution.

Phosphonates have three oxygen atoms capable of bonding to metals. They can also coordinate metals when they are in any state of protonation. This results in many possible modes of coordination and myriad different arrangements that the structures can take, many of which are not porous and therefore not MOFs. The majority of metal phosphonate compounds are not MOFs, and although there are a number of instances where phosphonate-based MOFs have been prepared, they were generally not by design. The interested reader is directed to a recently released book for more information.[8]

In addition to phosphonate-based MOFs, there is another classification of porous phosphonates that we refer to as unconventional MOFs, or UMOFs. These materials are poorly crystalline but show great thermal stability and are insoluble even in highly acidic media. They can also be pre- or post-synthetically functionalized and are finding uses as ion-exchange materials, proton conductors, catalysts, and sorbents. Whereas MOFs are highly crystalline and structurally well-characterized, UMOFs lack the highly ordered structures that define conventional MOFs. We will present some interesting observations on UMOFs and build a possible structural model that accounts for many of the observed phenomena. We shall necessarily discuss both MOFs and UMOFs in our coverage of porous materials based on phosphonate ligands.

Perhaps the first reported examples of UMOFs were a series of Zr compounds reported by Dines et al.,[9] which were based on biphenylbis(phosphonic acid) and methylphosphonic acid. His reasoning was that the methyl groups would alternate with the pillar biphenyl group in the space between the layers, creating porosity. The materials were indeed porous and exhibited a rather large range of pore sizes. The porosity increased with the

Special Issue: 2012 Metal-Organic Frameworks

Received: June 17, 2011
Published: November 29, 2011

dx.doi.org/10.1021/cr2002257 | *Chem. Rev.* 2012, 112, 1034–1054

amount of methylphosphonic acid used. However, Clearfield observed that even the compound that did not contain any methylphosphonate groups was almost as porous as the most porous of the biligand compounds.[10] With this observation as a beginning, researchers like Clearfield and Alberti pioneered further research into these families of porous materials.

This review will cover progress dating from 2005 until August 2011 for MOFs based on arylphosphonic acids and somewhat earlier for the alkylphosphonic acids. Most reviews have neglected to cover the latter type. We will mainly focus on MOFs made with derivatives of three main ligand types: alkylphosphonic acids, *N*,*N*′-piperazinebis(methylenephosphonic acid), and arylphosphonic acids. Some of these reports do not provide more than speculation into the nature of the porosity of the materials. We will do our best to report any significant sorption data, and we will refrain from speculation of porosity in those materials lacking appropriate data. In addition there needs to be an historical approach, so we will highlight significant papers (even though they may be included in other reviews) as a means to establish the underlying goals of research in the field of phosphonate MOF chemistry.

2. CONVENTIONAL PHOSPHONATE MOFS

Phosphonate-based MOFs are considerably rarer in the literature than their carboxylate-based counterparts. This is in part because phosphonates tend to form densely packed layered structures that are not porous. In addition, because of their lower solubility, metal phosphonates tend to be less crystalline than carboxylates. This often means that, even if one obtains a phosphonate-based MOF, it must be structurally characterized by powder X-ray diffraction (PXRD) instead of single-crystal methods. Also, phosphonates do not form the types of secondary building units with metal ions as the carboxylates do, so rational design of the target structures is nearly impossible. With these limitations being stated, there are three main classes of ligands that have been found to form phosphonate-based MOFs. These are alkylphosphonates, piperazinylphosphonates, and arylphosphonates.

2.1. Alkylphosphonate MOFs

The first 3D phosphonate framework containing open channels was reported in 1994 by Bujoli and co-workers where they had synthesized a $Cu(O_3PCH_3)$ containing 24-membered rings lined by pendant methyl groups as shown in Figure 1.[11] The pore size of this compound was too small (~3 Å) to incorporate any typical molecule used to characterize them. This framework was the first of its kind, although it was soon upstaged by the first zeolite-type phosphonates, α- and β-AlMePO ($Al_2(CH_3PO_3)_3$) reported in the subsequent months by Maeda and co-workers.[12−14] These materials contained trivalent aluminum cations in both tetrahedral and octahedral geometries with bridging phosphonate groups leaving hexagonal channels lined with methyl groups. Figure 2 shows the ~5 Å free diameter channels of both of these compounds. The nitrogen adsorption isotherms showed that the α-form had a two-step adsorption, whereas the β-form showed a type I isotherm. These materials are capable of taking up small gas molecules and hydrocarbons. Recently the α-form has been shown to be selective for ethyl chloride adsorption and could be used commercially as a scrubbing agent for polyvinyl chloride streams.[15] Although these findings laid the foundation for porous phosphonate research, they have been extensively covered in previous reviews and we will discuss them only as a means to provide a brief history.[16,17]

After the work of Maeda, the field expanded; recently there have been a few papers on the use of methylphosphonic acid with both scandium[18] and iron[19] to produce porous phosphonate frameworks, the latter of which exhibit interesting magnetic properties due to the inclusion of oxalate cross-linkers in the framework. The former contains charge-balancing sodium cations that are locked in a scandium framework and are unable to be removed. Aside from the work with methylphosphonic acid, the field was still in its infancy until the extension into alkylbis(phosphonic acids). In 1997, Lohse and Sevov reported a 3D open framework material with methylenebis(phosphonic acid) and cobalt(II) that contained 1D tunnels.[20] This sparked the plethora of work that has been done on methylenebisphosphonate materials, which included the stable nickel materials VSB-3 and VSB-4 reported by Férey and co-workers shown in Figure 3.[21] Recently there have been a few interesting actinide-based compounds such as the plutonium framework presented by Nelson and Albrecht-Schmitt in 2010[22] as well as some uranyl materials exhibiting interesting fluorescence.[22,23]

Upon increasing the chain length in alkylbis(phosphonic acids) of formula $(H_2O_3P(CH_2)_nPO_3H_2)$ (**C*n***) from $n = 1$ to $n = 2$, the structures change from dense layered motifs to open frameworks,[24,25] or in some cases even helical rods.[26] Merrill and Cheetham have reported many divalent and trivalent metal phosphonate frameworks synthesized with **C2**.[24,25] The trivalent metals yielded frameworks that were all dense and nonporous whereas the Co and Ni frameworks were isostructural to that of Zn presented by our group in 1997, which had elliptical channels running between the pillars of the ethylene groups.[27] This structure type has shown to be the predominant form for porous alkylbisphosphonates with chains lengths $n > 1$. We have shown with a number of divalent metals and chain lengths that the pillaring of the ligand often results in elliptical tunnels running along either the *a*- or *b*-axes.[27−30] This was first observed in a copper framework utilizing the **C3** ligand;[27] however, this was not uncommon for the vanadyl alkylbisphosphonates of the time.[31] It was speculated that the pore size may be controlled by varying the length of the alkyl spacer. Further investigations into the use of **C3** to **C5** produced both zinc and copper frameworks all containing unidirectional tunnels filled with solvent water that could be removed upon heating. In addition, some of these compounds contained coordinated water molecules that lined the pores and could be removed through heating, which would provide accessible metal coordination sites.[29] Unfortunately, due to the hydrophobic nature of the walls of the tunnel, after removal of the water, the channels are unable to be refilled.

The use of zinc in metal phosphonates often proves interesting as zinc easily adopts a number of coordination modes, namely, tetrahedral or octahedral, although five coordinate is not uncommon. Recently we have discovered that these zinc alkylbisphosphonates can be divided into several different families, each of which is based upon a different isoreticular structural archetype. The families will be referred to as zinc alkylbisphosphonate gate (ZAG), zinc alkylbisphosphonate cation (ZAC), and zinc alkylbisphosphonate tunnel (ZAT) compounds. First we will discuss several members of these families that have been previously reported by others.

In 2003 Rubibao Fu and co-workers presented a series of divalent phosphonates using **C4**.[32] In this paper, Fu reported the compound $Zn(HO_3P(CH_2)_4PO_3H)\cdot 2H_2O$ (ZAG-4) (Figure 4). This compound possesses a series of interconnected 1D inorganic chains creating 1D channels that contain both water molecules and protonated phosphonate groups. These groups produce an array of strong hydrogen bonds that holds the channel closed. The chains are made up of tetrahedrally coordinated zinc atoms that

dx.doi.org/10.1021/cr2002257 |*Chem. Rev.* 2012, 112, 1034–1054

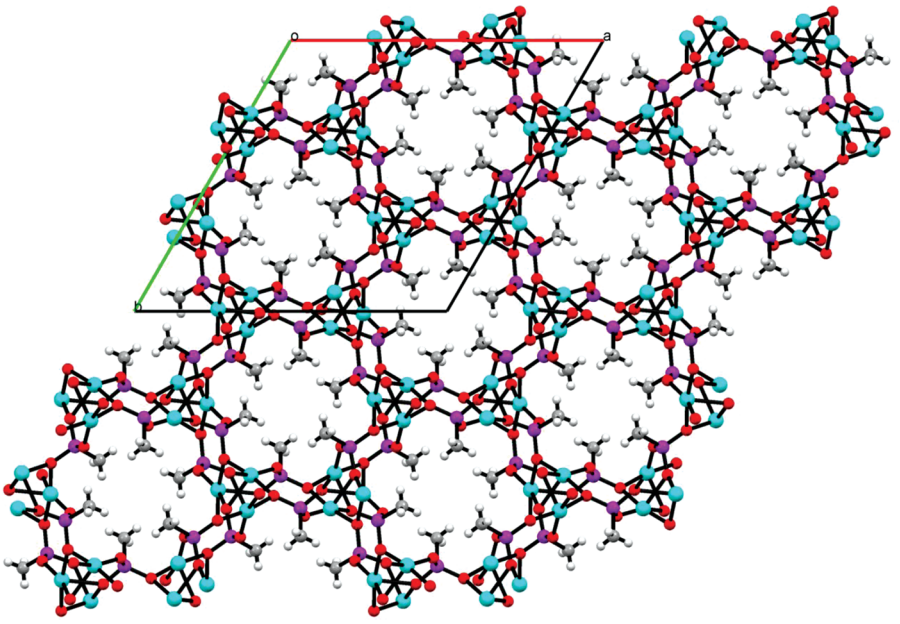

Figure 1. $Cu(O_3PCH_3)$ viewed along the *c*-axis showing the unidirectional tunnels lined with methyl groups. (C = gray, O = red, H = white, P = purple. *a* = red, *b* = green, *c* = blue. These conventions will be used for all structures.)

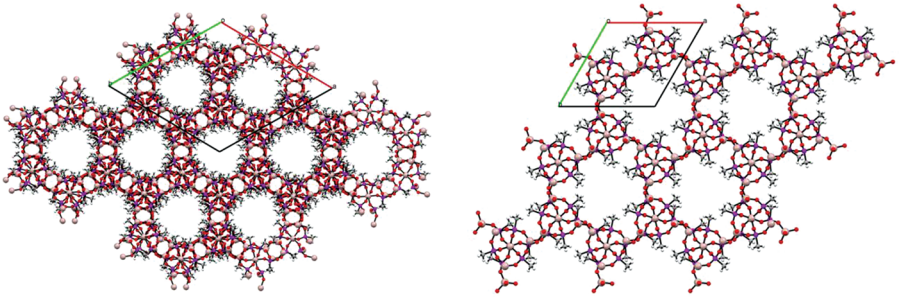

Figure 2. Showing the β-AlMePO (left) and α-AlMePO (right) as viewed down their respective *c*-axes.

bond to four phosphonate oxygen atoms, creating a line of 8-membered rings. In our own work (unpublished results), we have obtained the isoreticular compound $Zn(HO_3PC_6H_{12}PO_3H)\cdot 2H_2O$ (ZAG-6) (Figure 4), which has larger channels due to the longer alkyl chains separating the inorganic components. We hypothesize that the **C8** and **C10** members of this family may also exist, because they would have the same conformation of the alkyl linkers.

In similar work, using 2-methylpiperazine as a template, Fu and co-workers were able to obtain two related compounds $(C_5H_{14}N_2)Zn_4(O_3P(CH_2)_nPO_3)_2(HO_3P(CH_2)_nPO_3H)$ where n = 2 and 4.[33] The structures of these compounds contain a double layer of tetrahedrally coordinated zinc centers bridged by phosphonate linkages that connect to form 8-membered and 16-membered rings, which edge-share to form larger 24-membered rings. The double layers are cross-linked together by the alkylbis-(phosphonic acid), and the large 24-membered rings contain a fully protonated 2-methylpiperazine for charge balance. The structure contains two crystallographically distinct alkyl linkers, one which is fully deprotonated, and one which retains one proton per phosphonic acid. The fully deprotonated ligand is found in a normal straight-chain alkyl conformation; however, the other linker is distorted to a higher energy conformation. In our own work, we have synthesized the **C4** compound presented by Fu; however, the 2-methylpiperazine is replaced by a zinc hexaaqua cation and there are water and acetic acid molecules in the channels as well. By manipulation of the conditions for C4 and using C5 and C6, we have obtained the isoreticular compounds $Zn_4(O_3P(CH_2)_nPO_3)_2(HO_3P-(CH_2)_nPO_3H)Zn(OH_2)_6\cdot 4H_2O\cdot 2CH_3COOH$ where n = 4−6 (ZAC-4, ZAC-5, and ZAC-6, respectively). These new compounds contain the exact same inorganic structure as Fu's with the alkyl spacer simply extending the distance between the inorganic layers. Figure 5 provides a comparison between Fu's **C4** compound and our ZAC-6. In each of the different compounds there also exists the same distortion of the ligand that retains its protons. Between Fu's work and ours, it is reasonable to believe that these compounds may be able to incorporate a variety of different cations in the channels. This is currently being further explored.

The last family has been obtained recently by our group (unpublished results). These compounds contain 1D inorganic chains made of tetrahedrally coordinated zinc centers that are cross-linked in one direction by octahedrally coordinated zinc atoms and in the other direction by the alkyl linker. They have the formula $Zn_3(HO_3P(CH_2)_nPO_3H)(O_3P(CH_2)_nPO_3)(H_2O)_4\cdot xH_2O$

dx.doi.org/10.1021/cr2002257 |*Chem. Rev.* 2012, 112, 1034–1054

where n = 3 and 5 (ZAT-3 and ZAT-5, respectively). Figure 6 shows the network of tunnels in ZAT-5. The linkage of the chains forms tunnels of two different sizes; in ZAT-5 the larger of these tunnels has a free diameter of ~12.6 Å. Unfortunately ZAT-5 seems to collapse upon removal of the solvent waters, and surface area measurements on ZAT-3 have yet to be performed.

Similarly to our work with zinc, Zubieta and co-workers have reported a series of related vanadium compounds synthesized by systematically increasing the length of the alkyl spacers. They found that for n = 2, 3, 4, and 5 there are isoreticular structures in which the inorganic layers are identical, but the stacking between them varies slightly due to the conformation of the odd- or even-numbered chains.[34] After n = 5, the structural type changes to that of pillared slab structures from n = 6 to n = 8; and for n = 9 the structure obtained is a condensed double layer as shown in Figure 7. Although the construction of the vanadyl frameworks has been noticeably different from that of the later transition metals due to the bonded oxide, it is interesting to note the similarities between the n = 3−5 compounds for V and Cu (Figure 8). In the copper phosphonate structures, a water molecule takes the place of the vanadyl oxygen atom, resulting in a similar coordination environment.

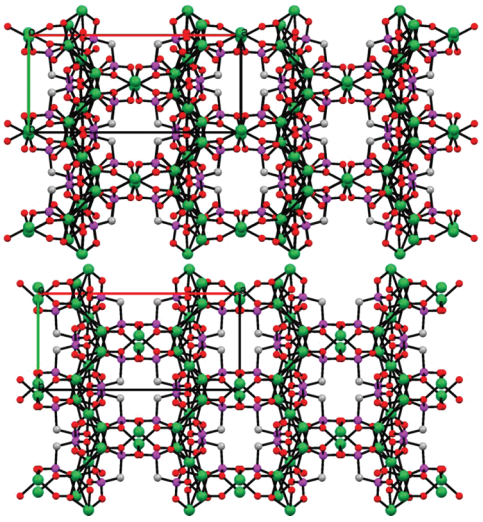

Figure 3. VSB-3 (top) and VSB-4 (bottom) viewed down their *c*-axes.

Attfield and co-workers recently reported a series of gallium alkylbisphosphonates in which they attempted to systematically vary the chain length from n = 3 to n = 10.[35] The results of their research combined with our own confirm that the structures of these compounds are quite diverse. However, identical reaction conditions can produce some materials that appear to be capable of isoreticular extension whereas others appear to be limited by the conformation of the ligands.

2.2. Piperazinylphosphonate MOFs

N,*N*′-piperazinebis(methylenephosphonic acid) is an interesting ligand as it contains two phosphonic acids, both capable of three total states of protonation, as well as two amino nitrogen atoms capable of two protonation states. This ligand and some of its derivatives are shown in Figure 9. The ligand can adopt one of several conformations, which adds to the versatility. The first compound using this piperazine-derived ligand was a nonporous vanadyl phosphonate reported by Zubieta and co-workers.[36] Shortly afterward they reported that the same ligand, when reacted with both Mn(II) and Co(II), yielded "porous" framework materials.[37] The structures were dense frameworks that contained small channels filled with solvent water molecules. Although the pores were capable of reversible hydration, the materials exhibited no permanent porosity. The most notable examples of piperazine-based phosphonates are STA-12[38] and MIL-91,[39] which have both been covered in previous reviews.[16] However, a brief description of these archetypal phosphonate MOFs is appropriate. A complete overview of this topic can be found in one chapter of the recently published book on metal phosphonates.[8]

$M_2(H_2O)_2(O_3PCH_2N(C_2H_4)_2NCH_2PO_3)$ (M = Mn^{2+}, Fe^{2+}, Co^{2+}, Ni^{2+}) (STA-12) is formed by 1D chains of edge-sharing MO_5N octahedra; the chain has pendant piperazinyl ligands that cross-link to form large hexagonal channels (Figure 10). The pores are lined by free P═O groups that extend into the cavity. The metals are all octahedrally coordinated by four phosphonate oxygen atoms, the nitrogen atom from the piperazine, and a water molecule. Upon dehydration, the structure distorts from rhombohedral symmetry to triclinic, and the final free diameter of the pore is ~0.8 nm. STA-12 was particularly interesting for three reasons.

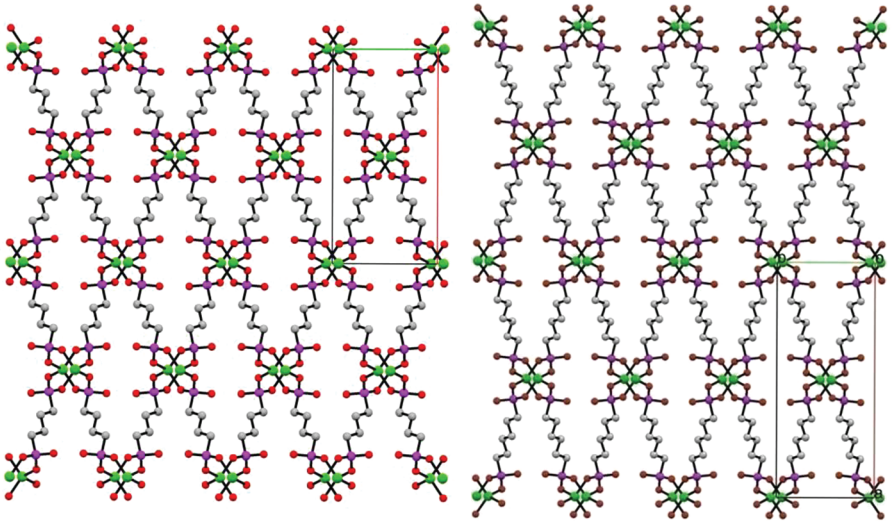

Figure 4. Comparison of ZAG-4 (left) and ZAG-6 (right) as viewed down their *c*-axes.

dx.doi.org/10.1021/cr2002257 |*Chem. Rev.* 2012, 112, 1034–1054

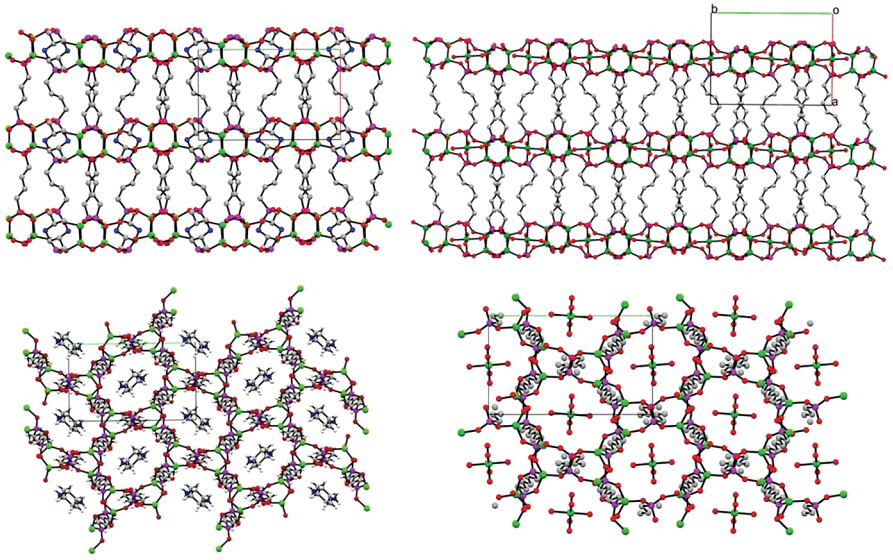

Figure 5. Fu's ZAC-4 compound containing 2-methylpiperazine cations (left, top and bottom) compared with ZAC-6 containing zinc hexaaqua cations (right, top and bottom).

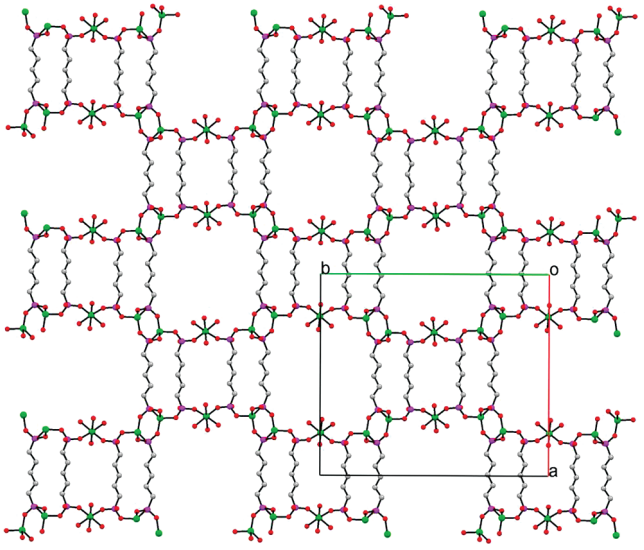

Figure 6. ZAT-5 viewed along the *c*-axis showing the open framework structure. Disordered solvent water molecules have been omitted for clarity.

First, upon dehydration the structure remains porous. Second, the pores are lined by pendant P═O groups, which can interact with gas or solvent molecules. Third, the water molecules bound to the metal centers can be removed, leaving coordinatively unsaturated Lewis acid sites. Wright and co-workers were able to solve the triclinic dehydrated structure and monitor the reversibility of the hydration/dehydration of the water bound at the metal site using synchrotron powder X-ray diffraction.[40] Furthermore, they used CO as a probe to analyze the Lewis acid characteristics of the material and showed that the CO adsorbs at both the metal sites and the pendant P═O sites. Interestingly, STA-12 showed much higher uptake of CO_2 than methane at 1 bar and 300 K (ΔH 30−35 vs 14−15 kJ mol^{-1}), which could be useful in separations.[40]

MIL-91, $MOH(HO_3PCH_2NC_4H_8NCH_2PO_3H)\cdot nH_2O$ (M = Al^{3+}, V^{3+}, In^{3+}, Fe^{3+}), has a porous structure (Figure 11) consisting of corner-sharing MO_6 octahedra linked together in two directions by the piperazinyl ligand.[8,39] This structure is also adopted by Ti^{4+} where $[TiO]^{2+}$ cations take the place of the $[MOH]^{2+}$ units in the trivalent structures. This connectivity creates 1D channels along the *b*-axis that are ∼4 Å in diameter that do not collapse upon the removal of solvent. The Langmuir surface area was determined to be ∼500 m^2/g.

We will now focus on some of the new and interesting derivatives that have been reported in the literature over the past few years. Because of the wide variety of coordination environments in lanthanides as well as their interesting magnetic and luminescent properties, they are attractive choices for building framework materials. A number of porous frameworks have been obtained from lanthanides and piperazinylbisphosphonates. Groves and co-workers reported a series of isostructural compounds utilizing Gd^{3+}, Y^{3+}, and Yb^{3+} that contain framework water molecules that can be removed reversibly without framework collapse.[41,42] They speculate upon the relationship between cation size and structural type, as Nd produced a different structure containing cross-linked lanthanide chains. Further increases in cation size (i.e., Ce^{3+}, La^{3+}) result in a new framework as well.[43] Addition of base to these reactions produces a different porous framework with La, Ce, and Nd that includes Na, K, or Cs cations.[43]

Mao and co-workers prepared mixed-ligand La and Nd phosphonate/sulfonates utilizing *N*,*N*′-piperazinebis(methylenephosphonic acid) and *para*-sulfonylphenylphosphonic acid. The structure contains hexagonal channels filled with solvent water that can be removed without structural collapse. However, no sorption measurements were performed to determine the porosity. Magnetic studies were carried out on the Nd compound, which showed strong antiferromagnetic interaction between metal centers.[44]

More recently, Wright and co-workers have expanded upon this system by incorporating new ligand designs, such as addition of methyl groups to the piperazine ring. In 2010 they reported the permanently porous lanthanide phosphonate framework STA-13, $M_2(HO_3PCH_2NC_5H_{10}NCH_2PO_3H)_3\cdot 7H_2O$ (M = Y^{3+}, Sc^{3+}, Yb^{3+}, and Dy^{3+}), which was synthesized from a racemic mixture of *N*,*N*′-2-methylpiperazinebis(methylenephosphonic acid).[42] The structure of STA-13 contains 1D M^{3+} phosphonate chains that

dx.doi.org/10.1021/cr2002257 |*Chem. Rev.* 2012, 112, 1034–1054

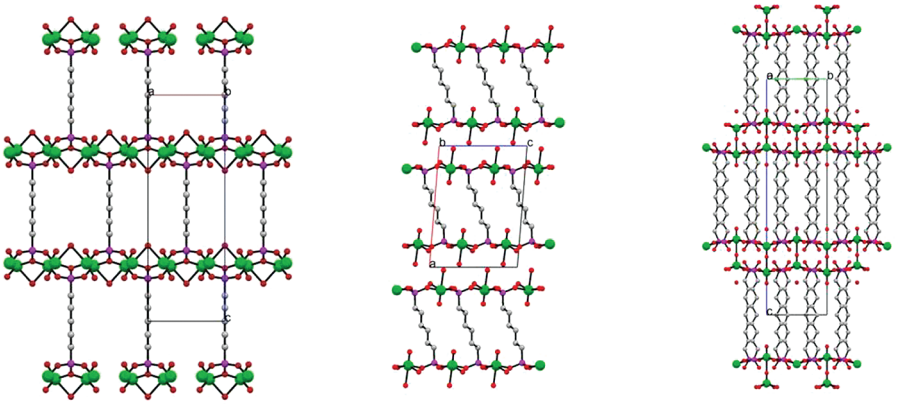

Figure 7. Three structural types reported by Zubieta of $V_2(O)_2(O_6P_2C_5H_{10})(H_2O)_4$ (left), $V_2(O)_2(O_6P_2C_6H_{12})(H_2O)_4$ (middle), and $V(O)(O_6P_2C_9H_{18})$ (right) viewed normal to their inorganic layers. Notice the progression from layer to double layer to condensed double layer from left to right. Solvent water molecules have been omitted for clarity.

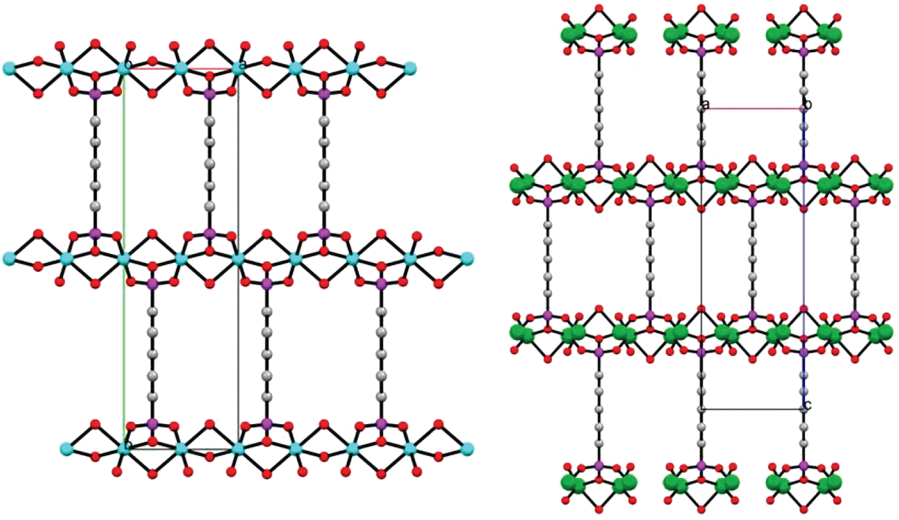

Figure 8. Comparison between $Cu_2[(O_3PC_5H_{10}PO_3)(H_2O)_2]\cdot 2.8H_2O$ (left) and $V_2(O)_2(O_6P_2C_5H_{10})(H_2O)_4$ (right). Although the structures are different, the overall topology is almost identical with shared oxo's in the vanadium structure being replaced by shared waters in the copper compound. All solvent water molecules have been omitted for clarity.

are connected through the bisphosphonate ligands to three other chains. This forms a hexagonal array of 1D tunnels along the *c*-axis filled with water molecules (Figure 12). Upon dehydration, the free diameter of these tunnels is ~3 Å with a pore volume of 0.12 cm^3/g. The use of the pure *R* enantiomer ligand results in a nonporous structure.[41] The researchers suggest that only the pure enantiomers are sterically capable of adopting the nonporous structure but the racemic mixture is not, and instead of producing a mixed-phase result, it instead forms the 3D porous framework STA-13.

Wright's group has also produced the isoreticular porous phosphonate MOF STA-16 (Figure 13), in which the use of *N*,*N*′-4,4′-bipiperidinebis(methylenephosphonic acid) was used to extend the wall size of STA-12 in a truly isoreticular expansion of the porous framework.[45] Isostructural species with Ni^{2+} and Co^{2+} were obtained and were determined to have pore volumes of 0.68 cm^3/g and pore diameters of ~1.85 nm.

In 2009, Costantino and co-workers reported the synthesis of a pillared layered Ce phosphonate containing bridging sulfate groups as well as 1D channels filled with hydrated water molecules. The

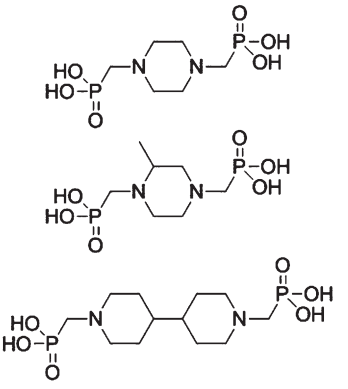

Figure 9. *N*,*N*′-piperazinebis(methylenephosphonic acid) (top), *N*,*N*′-2-methylpiperazinebis(methylenephosphonic acid) (middle), and *N*,*N*′-4,4′-bipiperidinebis(methylenephosphonic acid) (bottom).

water molecules can be removed, and the framework remains rigid up to 200 °C. No sorption studies were carried out on the material;

dx.doi.org/10.1021/cr2002257 |*Chem. Rev.* 2012, 112, 1034–1054

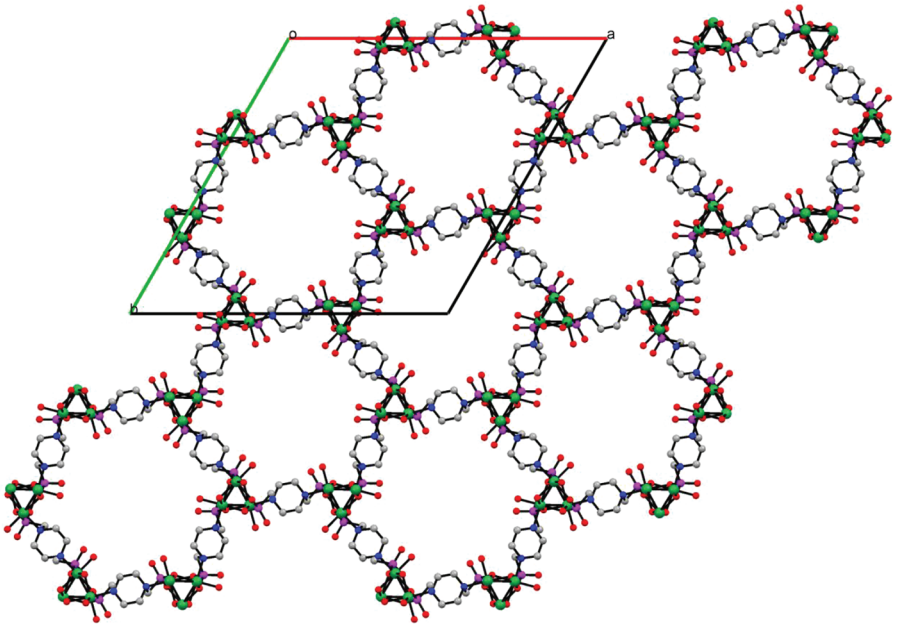

Figure 10. STA-12(Ni) as viewed down the *c*-axis showing the large hexagonal tunnels. Solvent water molecules have been omitted for clarity.

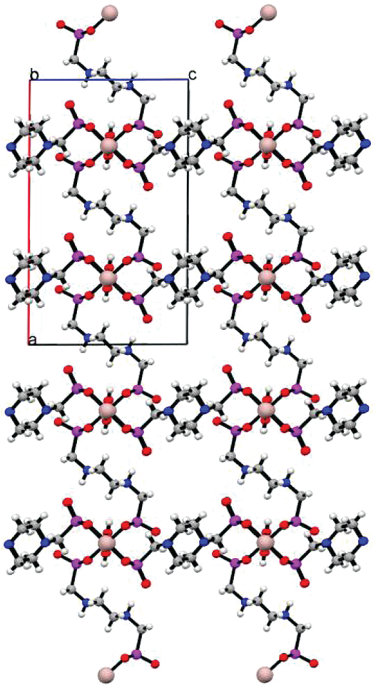

Figure 11. MIL-91(Al) as viewed down the *b*-axis. Solvent water molecules have been omitted for clarity.

however, it does show a luminescent band that is attributed to a charge transfer between the ligand and the Ce metal.[46]

Taddei and co-workers in Italy have recently reported two zirconium compounds with *N*,*N*′-piperazinebis(methylenephosphonic acid). The first structure exhibits 1D channels that can reversibly desorb and sorb water molecules (Figure 14). Unfortunately, the dehydrated material contracts and shows no permanent porosity. The second material has a pillared layered structure that

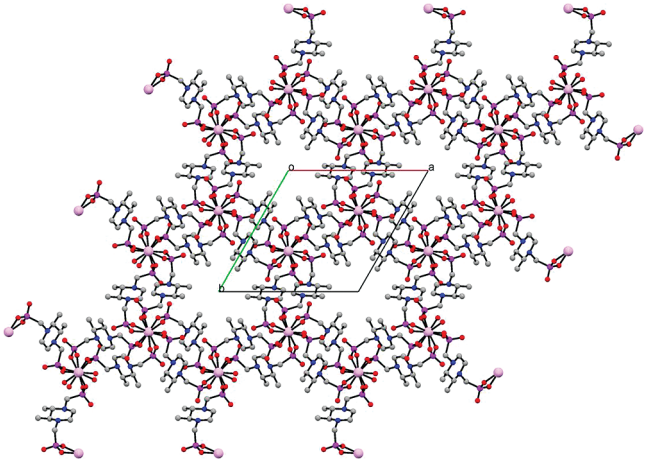

Figure 12. STA-13(Y) viewed down the *c*-axis. Solvent water molecules have been omitted for clarity.

contains bound fluoride ions, but the pillars are packed too closely to allow gas molecules into the structure.[47]

2.3. Arylphosphonate MOFs

Perhaps the first open-framework arylphosphonate compound was the tubular uranyl compound $UO_2(O_3PC_6H_5)\cdot 0.7H_2O$.[48] The structure was solved by PXRD. The uranyl ions have pentagonal bipyramidal coordination and are connected to each other, forming tubular 12-membered rings running down the *c*-axis. The structure is hexagonal as shown in Figure 15 with rings at the corners of the unit cell. The coordination resembles that in $Mn(O_3PC_6H_5)\cdot H_2O$, which is layered.[49] One phosphonate group chelates the U atom, and both chelating oxygen atoms donate an electron pair to adjacent U atoms, forming chains. The third oxygen atom of the chelating group bonds to a uranium atom above or below the first chain to form the wall of the tubules. The fact that

dx.doi.org/10.1021/cr2002257 |*Chem. Rev.* 2012, 112, 1034–1054

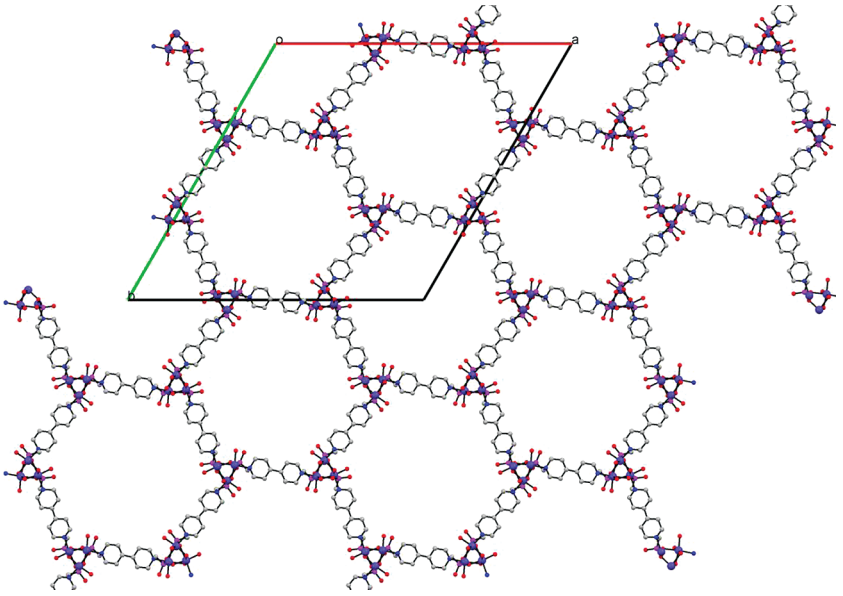

Figure 13. STA-16(Co) as viewed down the *c*-axis. Solvent water molecules have been omitted for clarity. Notice the similar connectivity to STA-12 in Figure 10.

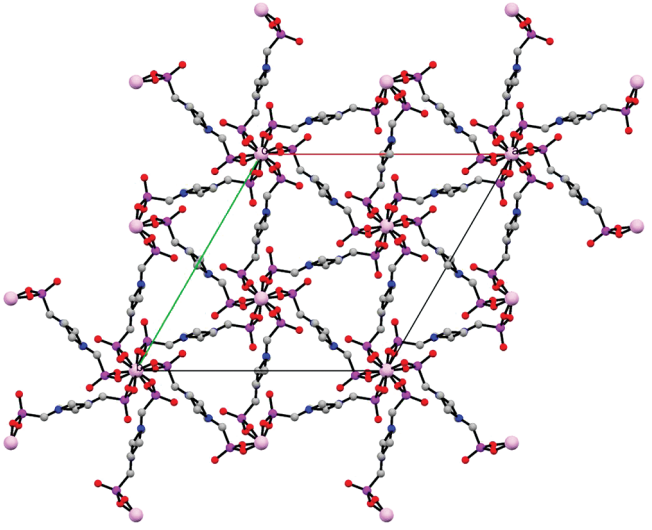

Figure 14. Zirconium *N*,*N*′-piperazinebis(methylenephosphonate) as viewed down the *c*-axis. Solvent water molecules have been omitted for clarity.

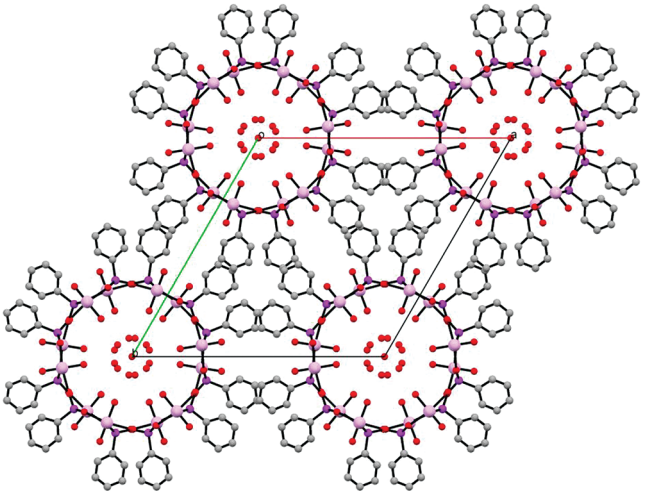

Figure 15. $UO_2(O_3PC_6H_5)\cdot 0.7H_2O$ viewed along the *c*-axis.

the uranyl oxygen atoms occupy the axial positions of the pentagonal bipyramid prevents layer formation. The phenyl rings are all on the outside of the tubes arranged around the 6-fold axes. The diameter of the 12-membered ring is 12.2 Å but the intrusion of U═O bonds into the interior of the tubules decreases the free space to ~7.3 Å. No surface area measurements were performed. It was also found that the two linear-chain uranyl phenylphosphonates could be easily transformed into the tubular one.[50]

A second tubular uranyl compound, $(UO_2)_3(HOPC_6H_5)_2(O_3PC_6H_5)_2\cdot H_2O$, was obtained upon refluxing a mixture of uranyl nitrate and phenylphosphonic acid for 30 days.[51] In this case the tubules are square, connecting four uranyl ions. All the phenyl rings again are on the outside. The tubule is not quite square, being 6.5 × 7 Å; however, since half the uranyl atoms are inside the tubules, there may be no free space. In this structure there are three independent U atoms, two of which are seven coordinate and one eight coordinate. Later, a polymorph of the original structure was discovered.[52]

It is well established that divalent metals typically form layered compounds when reacted with arylbis(phosphonic acids). The layers are pillared by the arylphosphonates, which are usually packed too closely together to allow gas or solvent molecules to pass between them, resulting in a stuffed, nonporous material. Even materials that are not layered are often nonporous, as the "voids" within the structures contain counterions.[53] However, there are clever strategies that allow for porous materials to be made. For instance, using a phosphonic acid with tetrahedral geometry that precludes the formation of layers has yielded good results.[54] This approach requires extensive ligand design and synthesis, so other tactics for inducing porosity may be more viable. The inclusion of a second, smaller phosphonate "spacer" ligand has been shown to produce porosity in tetravalent metal phosphonates, and this will be covered in a later section. Although it works well for Zr(IV) and Sn(IV), it often results in the formation of two phases when applied

dx.doi.org/10.1021/cr2002257 |*Chem. Rev.* 2012, 112, 1034–1054

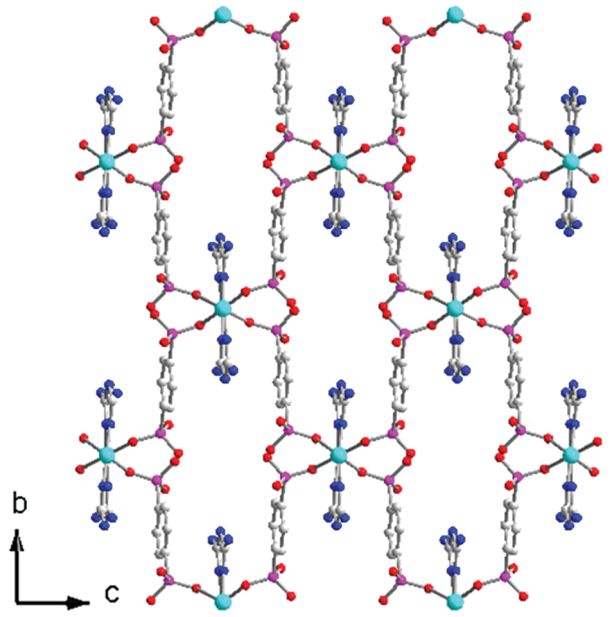

Figure 16. View of Cu(aminotriazole)($HO_3PC_6H_4PO_3H$) hydrate along the *a*-axis showing the open channels lined by amino groups.

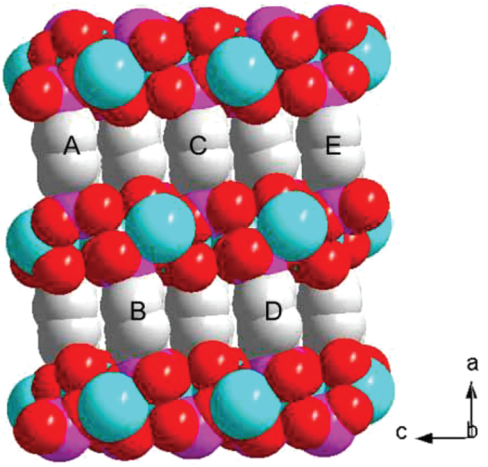

Figure 17. Space-filling model of the structure of Cu($HO_3PC_6H_4PO_3H$) hydrate. Replacing the ligands lettered A–E with aminotriazole ligands creates voids between the remaining phenyl rings, resulting in porosity.

to divalent metals. By using an aminotriazole coligand, Shimizu and co-workers were able to prepare a porous Cu compound with monophenylbis(phosphonic acid)[55] (Figure 16). This compound took up 0.5 mmol of CO_2/g and had a surface area of 69 m^2/g. The structure can be considered a derivative of the parent compound Cu($HO_3PC_6H_4PO_3H$)·H_2O (Figure 17), with every other column of phosphonate pillars removed, creating porosity. This approach may also work for biphenyl- or terphenylbis(phosphonic acids).

Zinc has been shown to make a variety of structurally distinct compounds with 4-carboxyphenylphosphonic acid (4-cppH_3) and various amines.[56,57] Many of these compounds that appear to be porous upon inspection of the crystal structure are actually not, as the pores or channels are filled by charge-balancing cations or solvent molecules that cannot be removed without the structure collapsing. Zheng and co-workers obtained the compound [Zn_8(4-cpp)$_6$(4,4′-bipy)][Zn(OH_2)$_6$], in which the charge of the anionic framework is balanced by hexaaqua zinc cations that occupy the channels running along the *c*-axis.[53] By using diazobicyclooctane (dabco) as a coligand, they were able to obtain the neutral, isostructural framework (dabcoH)$_2$[Zn_8(4-cpp)$_6$]·$6H_2O$, which contains only solvent water molecules within the channels. Unfortunately, the Brunauer–Emmett–Teller (BET) surface area of this compound after the removal of the solvent water is only 6 m^2/g.

The presence of solvent water within the pores of phosphonate-based MOFs may result in unique properties relating to proton conduction. The compound Zn_3(1,3,5-BTP)(H_2O)$_2$·$2H_2O$ (1,3,5-BTPH6 = 1,3,5-benzenetris(phosphonic acid)) was shown to have a low activation energy for proton transfer (0.17 eV).[58] The bulk conductivity of the material was not particularly high due to the fact that it is layered and conducts well only along the *ab* plane, which constrains intergrain proton transfer. However, it was shown by solid-state NMR (SSNMR) that the protons were freely mobile within the material down to −20 °C.

A similar phosphonate ligand, tris-1,3,5-(4-phosphonophenyl)-benzene (H_6L), was used by Vaidhyanathan et al. to synthesize the porous compound $Sr_2(H_2L)(CH_3OH)(H_2O)_4$, which was shown by uptake of CO_2 to have a surface area of 146 m^2/g even though the framework is interpenetrated.[59] Extending the arms of this ligand (or adamantane-based tetraphosphonic acids[54]) by including more phenyl spacers as a strategy for obtaining greater surface and larger pores is likely to be problematic, as the solubility of the ligand becomes an issue.

Phosphonate-based MOFs have distinct differences from carboxylate-based MOFs that make them attractive candidates for porous materials, namely, their thermal stability and extremely low solubility. However, this often makes it difficult to obtain single crystals, which can now routinely be used to determine the crystal structures. High-throughput hydrothermal techniques and advances in PXRD structure modeling and refinement will significantly increase the number of structurally characterized phosphonate-based MOFs, and it will be exciting to watch this field as it develops. It is likely that phosphonate-based MOFs will fill niche applications that are unsuitable for carboxylate-MOFs. There is an increasing number of mixed carboxylate–phosphonate MOFs, and these materials may serve to bridge the gap between these two types of MOFs, combining the most desirable attributes of each.

3. UNCONVENTIONAL PHOSPHONATE MOFS

Although the formal definition of a MOF is a source of some debate, it is generally agreed that they are hybrid organic–inorganic materials that are crystalline and porous. Yet there is another class of porous, hybrid materials that exhibits the general characteristics of a MOF, except for crystallinity. These materials are classified as unconventional MOFS, or UMOFs,[10] which are poorly crystalline, yet highly porous solids made from both organic and inorganic constituents. Many phosphonate-based materials fall into this category, because the poor solubility of phosphonate metal complexes results in rapid precipitation and poorly ordered structures, particularly for tri- and tetravalent metals. Phosphonate-based UMOFs exhibit high thermal stability and show great resistance to air and water. This allows them to be used or post-synthetically functionalized under conditions that would destroy other materials, while retaining their porosity. Although the potential

Table 1. Surface Areas of Aluminum Biphenylbisphosphonate Prepared in Alcohol−Water Solvents

		surface area (m^2/g)		
sample[a]	solvent[b]	total	external	micropore
49B	methanol/water	478.1	250.0	228.1
39A	ethanol/water	439.5	184.0	255.6
50B	butanol/water	343.3	230.2	113.1
50A	pentanol/water	352.8	264.9	87.9

[a] $AlCl_3 \cdot 6H_2O$/BPBPA = 8:3, T = 120 °C, 5 d. [b] 50:50 mix of alcohol−water.

Table 2. Surface Areas of Aluminum Biphenylbisphosphonate Phosphites

		surface area (m^2/g) (%)		
sample	Al/BPBP/H_3PO_3	total	external	micropore
51-A[a]	8:3:1.5	531.2	428.7 (80.7)	102.5 (19.3)
58-A[a]	8:3:1.5	361.0	263.4 (73.0)	97.63 (27.0)
58-A[d,a]	8:3:1.5	410.2	299.3 (73.0)	110.9 (27.0)
56-A[b]	8:1.5:1.5	611.2	571.0 (93.4)	40.25 (6.6)
51-B[a]	8:1.5:1.5	779.5	657.8 (84.4)	121.6 (15.6)
58-B[a]	8:1.5:1.5	389.3	331.0 (85.0)	58.28 (15.0)
56-B[c]	8:1.5:1.5	783.9	783.9 (100)	0.0 (0)

[a] 3:1 Ethanol/water. [b] 3:1 Methanol/water. [c] 3:1 Butanol/water. [d] Second preparation.

Table 3. Results of the BET Analyses of the Aluminum Biphenylbisphosphonate Phosphites

		surface area (m^2/g)		
sample	BPBP/H_3PO_3	total	external	micropore
150[a]	1:0	167.8	71.8	96.0
151[b]	1:2	294.4	107.1	187.3
152[c]	1:6	365.2	153.8	211.4

[a] Actual formula by elemental analysis: $Al_4[C_{12}H_8(PO_3)_2] \cdot 2.70H_2O$. [b] Actual formula by elemental analysis: $Al_4[C_{12}H_8(PO_3)_2]_{2.8}(HPO_3)_{0.4}$. [c] Actual formula by elemental analysis: $Al_4[C_{12}H_8(PO_3)_2]_{2.65}(HPO_3)_{0.7}(C_3H_6O)_{0.14}$.

applications of traditional phosphonate-based MOFs have been thoroughly investigated, the uses of UMOFs have not, although they show similar promise and great versatility. In this section we will cover UMOFs based on trivalent and tetravalent metals as well as strategies for obtaining porous materials and postsynthetically modifying them.

3.1. Aluminum Phosphonate UMOFs

Initial studies were carried out to determine the best ratio of Al^{3+} to biphenylbis(phosphonic acid) to obtain materials with the highest porosity. To our surprise the ratio turned out to be 8:3. This is similar to the results obtained for zirconium bisphosphonates where an excess of Zr^{4+} produced a narrower range of pore sizes.[60] Even with this ratio the products have a high level of external porosity as a fraction of total porosity. This fact is evident from the results in Table 1. Generally, with the tetravalent metal compounds, 90% or more of the pores are internal. We have found (in unpublished work) that aluminum bisphosphonate samples

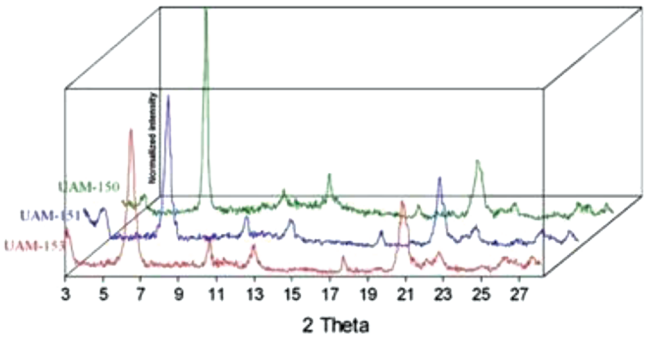

Figure 18. Powder X-ray diffraction pattern for sample UAM-150. Adapted with permission from ref 63. Copyright 2006 Springer Science + Business Media.

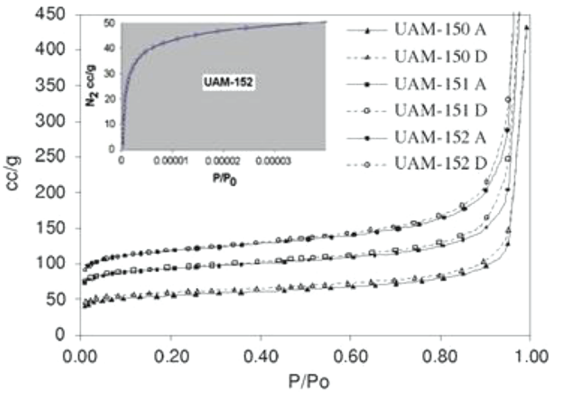

Figure 19. Nitrogen sorption/desorption isotherms of various aluminum biphenylbisphosphonates. Adapted with permission from ref 63. Copyright 2006 Springer Science + Business Media.

prepared in methanol−water or ethanol−water mixtures typically have more internal porosity, but even these are low relative to M(IV) bisphosphonates.

We thought to increase the internal porosity by addition of the spacer O_3PH through use of phosphorous acid. The results collected in Table 2 are interesting although disappointing. Very high surface areas were obtained but with very low levels of internal porosity. In the case of the compound prepared in a mixture of butanol and water, there was no internal porosity. For this to be realistic, the particles must be extremely small with few layers and rough surfaces. For example, the surface may be covered with separate regions of high concentrations of either bisphosphonate or phosphite, resulting in a topographical roughness that could greatly increase the external surface area.

In the next set of trials, carried out collaboratively in Spain, the temperature was increased to 185 °C for 7 days using a 1:1 mixture of acetone and water.[61] The results collected in Table 3 show a systematic increase in the amount of phosphite incorporated and a corresponding increase in surface area;[61] however, the amount of phosphite incorporated is much less than is present in the initial mixture. The X-ray pattern for sample UAM-150 is shown in Figure 18. The first peak, at 26.6 Å, is weak, while the second peak at 13.3 Å is strong. It is clear that these peaks are 001 and 002, respectively (assuming the layer lies in the *ab* plane). Undoubtedly the intense peak is due to the interlayer distance but the true unit cell extends to double that distance. This may result from the

dx.doi.org/10.1021/cr2002257 |*Chem. Rev.* 2012, 112, 1034–1054

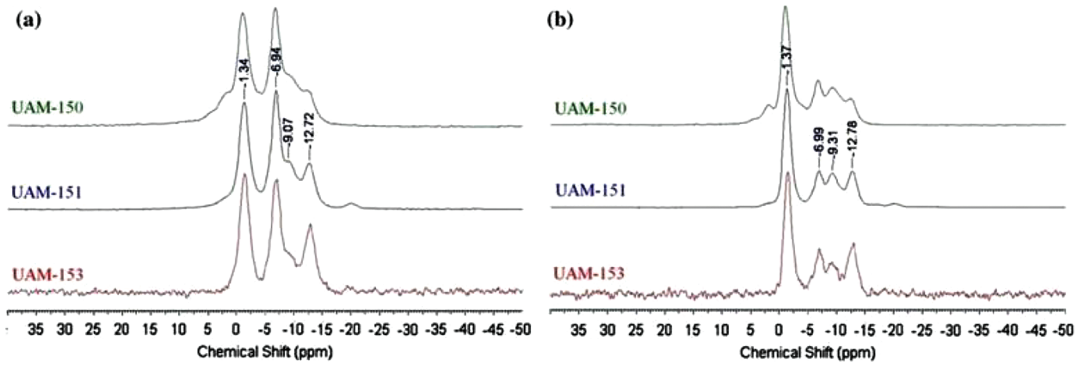

Figure 20. CP (a) and non-CP (b) MAS ^{31}P-NMR spectra of the indicated materials. Adapted with permission from ref 63. Copyright 2006 Springer Science + Business Media.

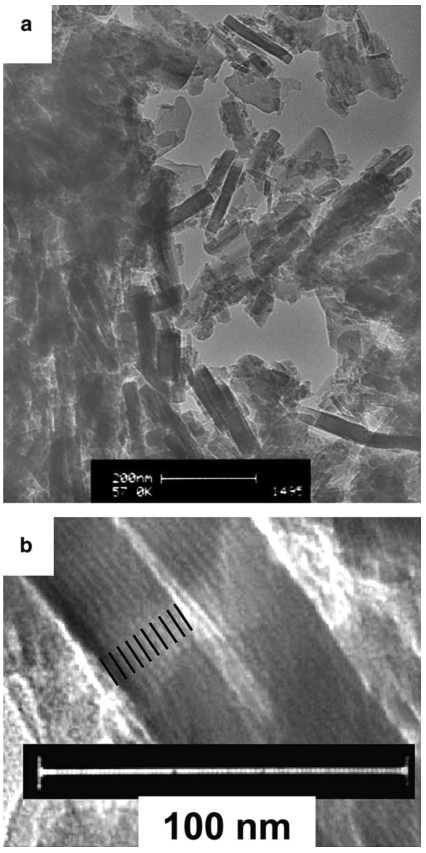

Figure 21. Transmission electron microscopy (TEM) images of aluminum biphenylbisphosphonates. The lower image clearly shows the interlayer spacing. Adapted with permission of from ref 63. Copyright 2006 Springer Science + Business Media.

canting of the pillars in different directions in adjacent layers. The isotherms shown in Figure 19 are type I with negligible hysteresis, indicative of a lack of mesopores. Analysis of the isotherm showed a bimodal pore size distribution with maxima at 6 and 15 Å. These aluminum phosphonate−phosphites also showed a fairly high uptake of H_2.[61]

The complexity of these structures is indicated by the solid-state magic-angle spinning (MAS) NMR results. All three samples exhibited a sharp resonance for ^{27}Al at 46.5 ppm and a broad singlet (or an unresolved doublet) at ∼−20.7 ppm. These shifts can be

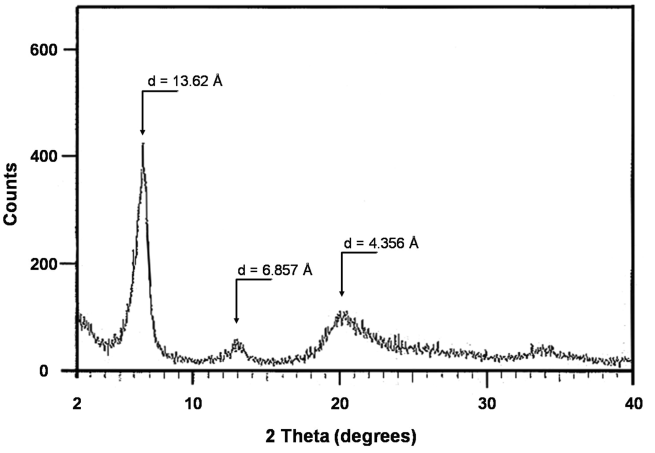

Figure 22. X-ray diffraction powder pattern of zirconium biphenylbisphosphonate.

attributed to four-coordinate and six-coordinate ^{27}Al. The MAS ^{31}P spectra with and without applying cross-polarization (CP) are shown in Figure 20. The CP spectrum of compound UAM-150, containing no H_3PO_3, exhibited two resonances at −1.34 and −6.94 ppm and two weak overlapping resonances of about 1/3 height. The non-CP spectrum shows a reduced peak at −6.94 ppm at the same level as the two weak resonances. Both the PXRD patterns and the NMR spectra for UAM-151 and UAM-152 indicate that the framework remains essentially intact in the mixed phosphonate−phosphite as compared to the pure phosphonate. Furthermore, the ^{27}Al NMR spectra are similar to those recorded for the compounds $Al_2(O_3PR)_3 \cdot 2H_2O$.[12] A compound with this formula (R = C_6H_5) was also synthesized by Cabeza et al.[62] for which the first intense reflection in the PXRD pattern was ∼13.0 Å. This would indicate a layered compound in which the interlayer spacing is 13.0 Å and a bilayer of phenyl groups exists between the layers. From the ^{27}Al MAS NMR spectra's similarities to that of AlMePO, it can be concluded that the coordination environment of the aluminum atoms in the UAM-150 type compounds must be very similar, but the structure has not yet been determined.

Aluminum biphenylbisphosphonates have been prepared under a variety of conditions, some of which contributed to extensive hydrolysis of the aluminum phosphonate layers.[63] This paper also includes examination of phenylphosphonate as a spacer for the biphenyl pillars. Figure 21 shows the particle size of a sample of composition $Al(O_3PC_{12}H_8PO_3)_{0.75} \cdot 1.5H_2O$. It was prepared in a

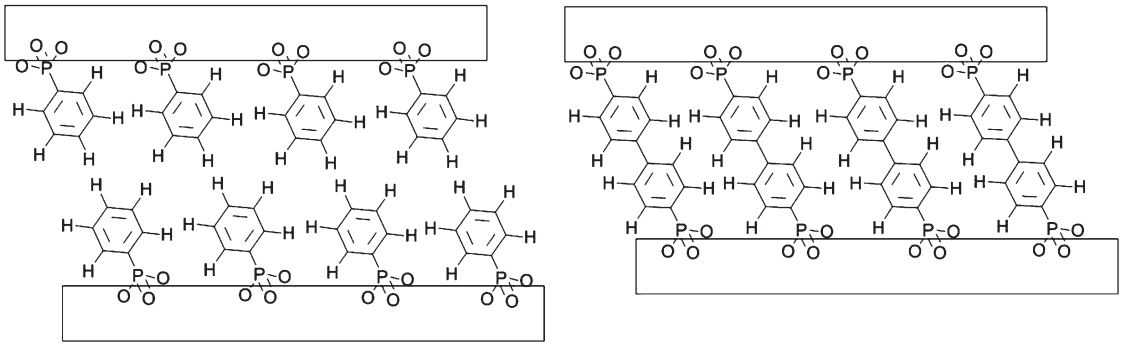

Figure 23. Illustration showing ideal structures of zirconium phenylphosphonate and zirconium biphenylbisphosphonate.

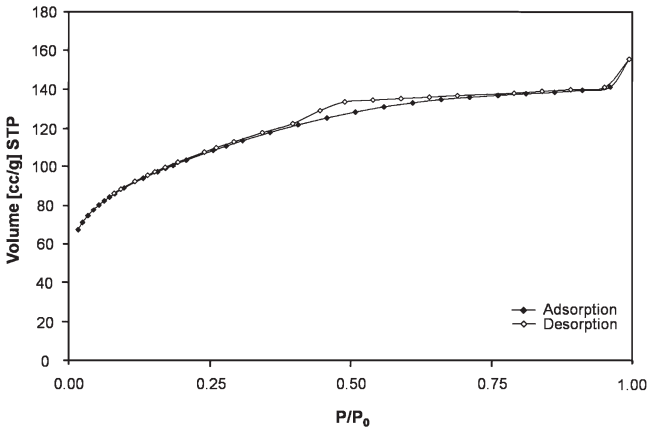

Figure 24. Representative N_2 adsorption (♦)−desorption (◊) isotherms obtained at 77 K for zirconium biphenylbisphosphonate prepared in DMSO.

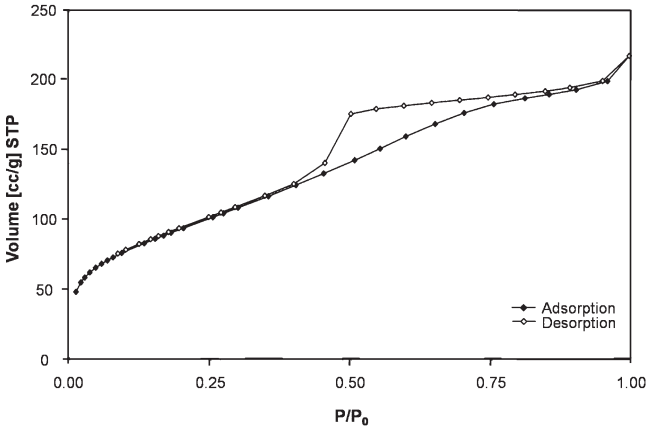

Figure 25. N_2 sorption−desorption isotherms for zirconium biphenylbisphosphonate prepared in ethanol at 80 °C for 3 days.

mixture of dimethyl sulfoxide (DMSO)−H_2O with an Al/P ratio of 4:6. The figure shows particles with nine layers with an interlayer spacing of 27.7 Å. The PXRD pattern features an intense peak at 13.9 Å, probably the 002 reflection. The BET surface area of this compound is 296 m^2/g, of which 252 m^2/g is internal (as shown by the t-plot method). The isotherm is a type I with an H4 hysteresis loop (IUPAC system),[64] indicative of slit-shaped pores

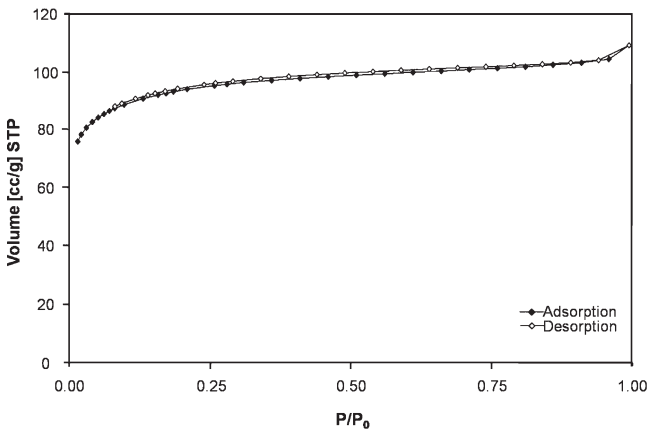

Figure 26. Zeolite-like N_2 sorption−desorption isotherm for the mixed derivative $Zr(O_3PC_{12}H_8PO_3)_{0.5}(O_3PCH_3)$.

of uniform size. A sample prepared in pure DMSO yielded a solid with a type I isotherm and a lower porosity of 146 m^2/g. It may be that the significant amount of hydrolysis that occurs in the samples prepared in mixtures of DMSO and water serves to introduce defect sites within the layer, which effectively spaces the phosphonate pillars apart, resulting in higher porosity.

3.2. Zirconium Phosphonate UMOFs

As previously indicated in the Introduction, the fact that $Zr(O_3PC_{12}H_8PO_3)$ was shown to be porous by Dines et al.,[9] even when no small spacer molecule was present, aroused our curiosity. Dines' intent was to prepare catalysts in which the porosity would be tunable. Several other papers on the subject of porous pillared zirconium materials have been published.[30,60,65]

The compounds reported by Dines showed a wide distribution of pore sizes. In an effort to design a porous phosphonate with more regular pores, Alberti et al.[66] prepared a Zr compound based on 3,3′,5,5′-tetramethylbiphenylbis(phosphonic acid). Because of the methyl groups on the phenyl rings, the pillars cannot take positions on the layer adjacent to one another. Including a small ligand such as phosphate or phosphite to occupy every other position on the layer resulted in the pillars being spaced ∼10 Å apart. The surface area was 375 m^2/g and the pore size maximum was 6.0 Å in diameter, which is close to what would be expected based on the distance between the pillars.

Our procedure for preparing Zr-based UMOFs is by hydrothermal or solvothermal techniques. As soon as the solution of $ZrOCl_2 \cdot 8H_2O$ is mixed with the phosphonic acid, a fine white

dx.doi.org/10.1021/cr2002257 |*Chem. Rev.* 2012, 112, 1034–1054

Table 4. Effect of Solvent on the Porosity of Zirconium Biphenylbisphosphonate−Monophenylphosphonate in Ratio Zr/BPBP/PhP = 1:0.25:0.5, T = 80 °C, t = 3 Days

	solvent			micropore		
sample no.	DMSO	ethanol	total SA/m^2g^{-1}	SA/m^2g^{-1}	max (range)/Å	vol./cm^3g^{-1}
1−1	17.5	0.0	421	395.0	13 (7−20)	0.175
1−2	14.0	3.5	323	305.0	12 (7−20)	0.149
1−3	10.5	7.0	311	295.0	11−13 (8−21)	0.169
1−4	7.0	10.5	324	303.0	12 (5−20)	0.164
1−5	3.5	14.0	396	331.0	15, 20	0.293
1−6	0.0	17.5	336	293.0	18 (9−22)	0.238

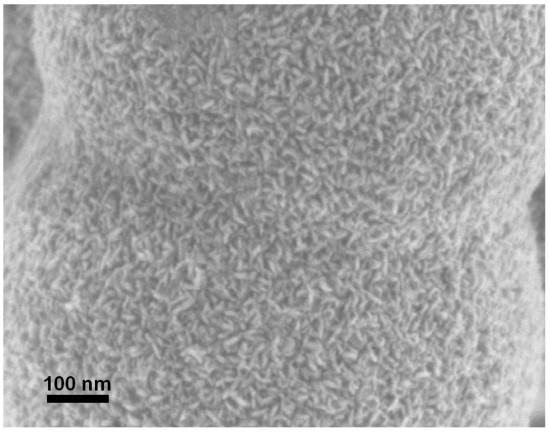

Figure 27. TEM image of $Sn(O_3PC_6H_5)_2$ showing the globules formed by the house-of-cards arrangement of the nanoparticles.

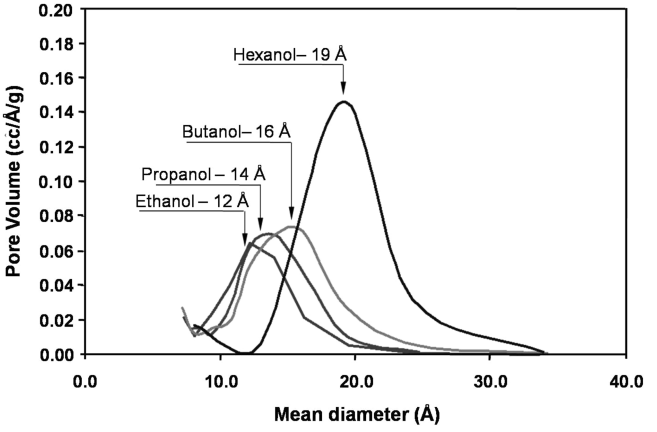

Figure 29. Pore size distributions for Sn(4-(4′-phosphonophenoxy)-phenylphosphonate) in alcohol/water mixed solvents.

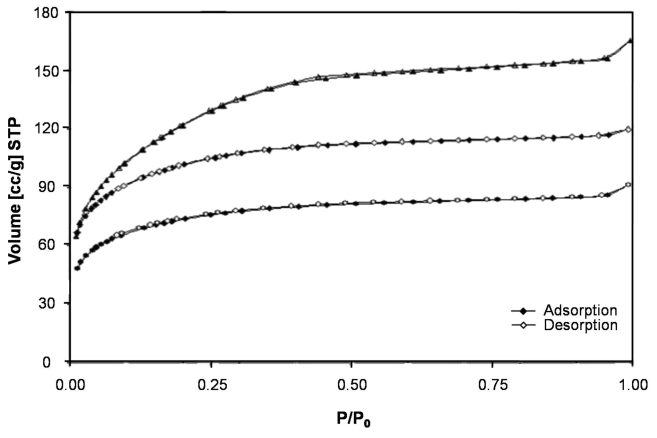

Figure 28. N_2 sorption−desorption isotherms for Sn(IV) biphenylbisphosphonate−monophenylphosphonates, $Sn(O_3PC_{12}H_8PO_3)_{1-x/2}(O_3PC_6H_5)_x$; x = 0, sorption ♦, desorption ◇; x = 0.666, sorption ●, desorption ○; x = 1.33, sorption ▲, desorption Δ.

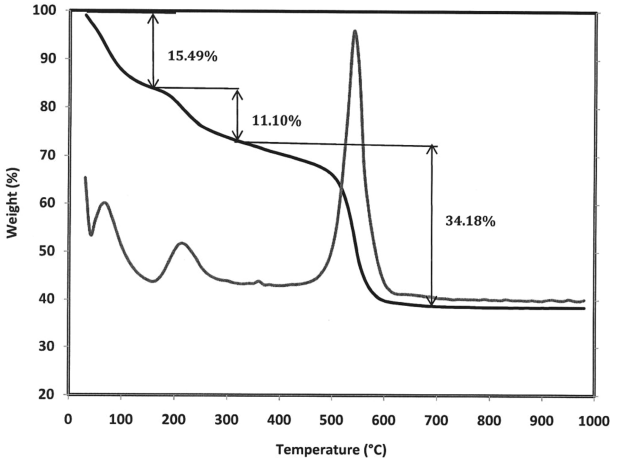

Figure 30. TGA curve for highly sulfonated Zr biphenylbisphosphonate with formula weight 676 g/mol for $Zr(O_3PC_{12}H_8PO_3)(SO_3)_{2.1}\cdot 5.8H_2O$.

powder forms. This powder is almost completely amorphous. When DMSO is used as the solvent, the temperature is held at 80−100 °C for three days. Higher temperatures are used when the reactions are performed in alcohol and alcohol−water mixtures. A typical PXRD pattern is shown in Figure 22. It is evident that the structure cannot be derived from such a poor pattern; however, there is some information to be gained from a pattern like this. The first peak is 13.62 Å and is assigned to the interlayer distance. Our justification for this choice uses the structure of the phenylphosphonate, $Zr(O_3PC_6H_5)_2$, as a model. It has a layered structure with an interlayer distance of 14.82 Å.[67] The inorganic portion of the layer has the same composition as that of α-zirconium phosphate,[68,69] $Zr_2O_6P_2$ (formula $Zr(O_3POH)_2$), except that the pendant −OH groups of the phosphate are replaced by a bilayer of phenyl groups in the interlayer space. In the case of the

dx.doi.org/10.1021/cr2002257 |*Chem. Rev.* 2012, 112, 1034–1054

Table 5. Synthetic Conditions and BET Surface Areas of Zr Bipyridyl/Methylphosphonates

	initial reaction mixture							
sample name	$ZrOCl_2 \cdot 8H_2O$ (mmol)	bpyBPAE (mmol)	MePA (mmol)	ratio Me/bpy	HCl (mmol)	reaction conditions	surface area (m^2/g)	percent micropores
Zr1	0.5	0.125	0.75	6:1	3	120 °C, 3 days		
Zr2	0.5	0.167	0.67	4:1	3	120 °C, 3 days		
Zr3	0.5	0.25	0.5	2:1	3	120 °C, 3 days	528	93
Zr4	0.5	0.33	0.33	1:1	3	120 °C, 3 days	472	92
Zr5	0.5	0.375	0.25	2:3	3	120 °C, 3 days	462	92
Zr6	0.5	0.5	0	0:1	3	120 °C, 3 days	353	96

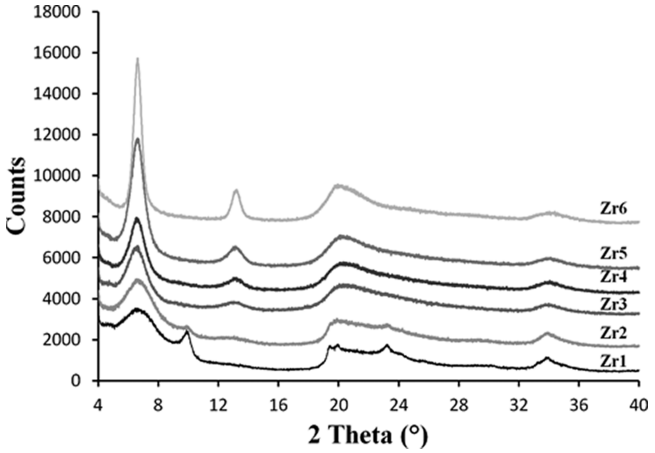

Figure 31. PXRD patterns of Zr-based phosphonates described in Table 5.

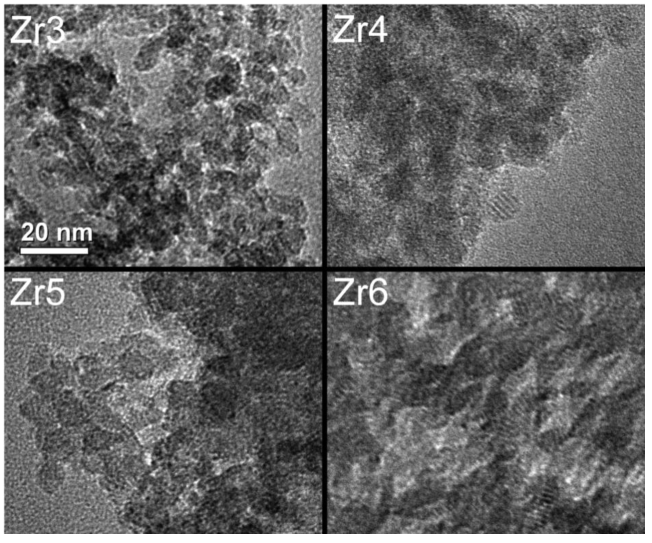

Figure 32. TEM images of compounds **Zr3**−**Zr6** showing the increase in particle size as less methylphosphonate spacer is incorporated.

biphenyl derivative, the biphenyl groups cross-link the layers. The increased distance for the phenyl derivative is due to the van der Waals gap (Figure 23). If this was all that there was to the structure, we might expect a semicrystalline compound with the pillars ~5.3 Å apart. In such a case there should be no porosity. However, the porosity varies from 250 to 400 m^2/g depending upon the solvent utilized, the temperature, and the time of heating. Porosities are determined from N_2 sorption−desorption isotherms run at 77 K and analyzed by the BET method. Another piece of information we may derive from the PXRD pattern is that the peaks are relatively broad, indicative of small particle size. In fact, as we shall show later, they are nanosized. In spite of that, most of the pores are internal and have diameters in the range of 10−20 Å.

Typical isotherms for $Zr(O_3PC_{12}H_8PO_3)$, zirconium biphenylbisphosphonate (Zr BPBP), are shown in Figures 24 and 25. Zr BPBP prepared in DMSO exhibits an isotherm that is more like a type I with a small hysteresis loop. The bulk of the N_2 is adsorbed below a P/P_0 value of 10^{-3} atm. The high level of N_2 sorption shown at this pressure indicates that a large percentage of the pores are <15 Å in diameter. The subsequent curvature and slight hysteresis loop indicate a range of pore sizes. Utilizing the t-plot method, the maximum in the pore size histogram is centered at 12 Å with a much smaller peak at 21 Å. The total surface area is 370 m^2/g, with 358 m^2/g internal and a pore volume of 0.198 cm^3/g. In contrast, Figure 25 shows the isotherm obtained using largely alcohol or alcohol/DMSO. The hysteresis loop is quite large as is the steepness of the slope over the full range of the curve. This behavior is more like a type IV isotherm in the IUPAC classification, which indicates a broad distribution of pore sizes.

Although most of our work has been concentrated on the biphenyl-pillared derivatives, we have also prepared porous products with monophenyl and terphenyl pillars. The interlayer spacings are 9.6 and 18.5 Å,[70] respectively. As shown by the work of Dines[9] and Alberti,[66] the pillars can be spaced apart by the inclusion of a small ligand. Dines used phosphate groups as the spacer, whereas Alberti used phosphite groups. This method for creating UMOFs depends on the rapid precipitation of the two ligands with Zr to form a single phase. If the temperature of the reaction is too high, the solubility of the product is increased and two separate phases will form. This is the case for almost all the simple monovalent and divalent metal phosphonates, so this strategy is limited to trivalent and tetravalent metal phosphonates. Some interesting findings have developed from our studies, and it is worth going into some detail in describing mixed-ligand phosphonate UMOFs.

We will first consider use of methylphosphonic acid as the second ligand. We have found that the type of nitrogen sorption isotherm obtained depends upon the amount of methyl groups incorporated. At low levels of methylphosphonate (0.7:1), the isotherms resemble those in Figure 24. However, at ratios greater than 1:1, the isotherms become more zeolite-like, that is, more like type I, as shown in Figure 26. This isotherm indicates a much more regular pore structure with almost all the pores being smaller than ~10 Å in diameter. The surface area is 334 with 325 m^2/g as micropores. A similar terphenyl derivative yielded a surface area of 540 with 527 m^2/g from micropores.

dx.doi.org/10.1021/cr2002257 |*Chem. Rev.* 2012, 112, 1034–1054

Table 6. Synthetic Conditions and BET Surface Areas of Sn(IV) Bipyridyl/Methylphosphonates

	initial reaction mixture							
sample name	$SnCl_4 \cdot 5H_2O$ (mmol)	bpyBPAE (mmol)	MePA (mmol)	ratio Me/bpy	HF (mmol)	reaction conditions	surface area (m^2/g)	percent micropores
Sn1	0.5	0.125	0.75	6:1	8	140 °C, 3 days	515	77
Sn2	0.5	0.167	0.67	4:1	8	140 °C, 3 days	434	80
Sn3	0.5	0.25	0.5	2:1	8	140 °C, 3 days	388	85
Sn4	0.5	0.33	0.33	1:1	8	140 °C, 3 days	363	85
Sn5	0.5	0.375	0.25	2:3	8	140 °C, 3 days	357	85
Sn6	0.5	0.5	0	0:1	8	140 °C, 3 days	323	82

Another group of interesting mixed-ligand materials is obtained by the use of phenylphosphonic acid as the spacer ligand. The phenyl group was chosen for two reasons. It will be remembered that the pure zirconium phenylphosphonate has a larger interlayer spacing than Zr BPBP (Figure 23) and the phenyl rings are tilted 30° to the perpendicular. Therefore, they may be unable to fit between the pillars. The second reason is that, even if the phenyl groups can fit, the surface area and porosity should decrease drastically. The effect of solvent on a mixed-ligand phenyl−biphenyl derivative is shown in Table 4. In this data set we see that, in spite of the change in solvent, the total surface areas are high, and there is only a slight diminution in the percentage of micropores to total porosity. Furthermore, the pore size range and micropore volume are not substantially different than that measured for the methyl mixed derivative materials. The implication of these results on an initial model of the structures of our Zr phosphonates will be taken up after we describe some other UMOFs.

3.3. Tin(IV) Phosphonate UMOFs

Mal et al. prepared tin phenylphosphonate, $Sn(O_3PC_6H_5)_2$, and found that when prepared in the presence of sodium dodecyl sulfate (SDS) it was microporous,[71,72] but in the absence of SDS it was mesoporous with a broad distribution of pore sizes.[73] Our preparation was also porous, but electron microscopy revealed an interesting type of porosity.[74] The tin phenylphosphonate formed micrometer-sized spherical particles. High-resolution scanning electron microscopy (SEM) (Figure 27) revealed that the individual particles were nanosized platelets forming a house-of-cards type porosity.[75] Even ligands with functional groups such as carboxylates formed porous architectures of this type. Addition of NH_4OH to $Sn(O_3PCH_2COOH)_2$ resulted in colloidal dispersion of the particles. In the presence of 30% H_2O_2, these porous phosphonates act as catalysts for the Baeyer−Villiger oxidation reaction.[76] These reactions involve the oxidative cleavage of a carbon−carbon bond adjacent to a carbonyl that converts ketones to esters and aldehydes to alcohols. An advantage with our catalyst is that the reactions are carried out in water, avoiding the use of organic solvents. Mixed derivatives of the type $Sn(O_3PC_6H_5)_x(O_3PCH_3)_{2-x}$ with enhanced porosity were also prepared.[75]

We have prepared $Sn(O_3PC_6H_4PO_3)_{0.5}(O_3POH)$ and the sodium phase of this material, as well as the biphenyl and terphenyl bisphosphonate analogues.[77] Similarly to the corresponding Zr compounds, the monophenylbisphosphonates were characterized by type I sorption−desorption isotherms, but those for the biphenyl derivatives were type IV. The pore structure depended upon the choice of solvent. Synthesis in water−alcohol mixtures yielded products with surface areas ranging from 322 to 442 m^2/g with a broad distribution of pores from 9 to 22 Å in diameter with a maximum at ∼16 Å. However, carrying out the reaction in a $DMSO/H_2O$ mixture yielded a product with a type I isotherm and 385 m^2/g with internal porosity of 378 m^2/g and a peak in the pore size distribution at 9 Å diameter.[10]

Like the zirconium compounds, the mixed Sn(IV) biphenylbisphosphonate−phenylphosphonate hybrid of general composition $Sn(O_3PC_{12}H_8PO_3)_x(O_3PC_6H_5)_{2-2x}$ shows a type I isotherm (Figure 28).[10,77] These curves show clearly that the pores are larger than the interlayer spacing. The tin biphenylbisphosphonate interlayer spacing is 13.8 Å but the layer thickness is 6.6 Å, leaving a free space of 7.2 Å. However, the average pore diameter obtained from the isotherms is 9−11 Å.

In a change of pillar, the 4-(4′-phosphonophenoxy)phenylphosphonic acid (PPPA) ($H_2O_3PC_6H_4-O-C_6H_4PO_3H_2$) was prepared to use as a cross-linker for the Sn(IV) derivatives.[78] Highly porous pillared compounds were prepared using this cross-linker. We note that these preparations were carried out in mixed solvents that controlled the nature of the N_2 isotherm and the pore size. The average pore size increased as a function of the size of the alcohol portion of the solvent. This fact is illustrated in Figure 29. It should be interesting to determine how far this control of pore size can be carried. If the pore sizes can be predetermined to yield pores below 10 Å to sizes in excess of 20 Å, a number of important applications should become apparent.

3.4. Functionalization of Phosphonate UMOFS

There is a long history in sulfonating zirconium phenylphosphonate and studying its properties as a Brønsted acid catalyst and proton conductor. Sulfonation is effected in fuming sulfuric acid[79] or by using chlorosulphonic acid. The sulfonated material is an excellent proton conductor[80] and, as a Brønsted acid, was shown to have the same acid strength as 100% H_2SO_4.[60] In the case of Zr BPBP, it was possible to achieve a sulfonation level of 1.1 $-SO_3$ units per phenyl ring and to retain most of the $-SO_3$ groups at 250 °C. The thermogravimetric analysis (TGA) of this sulfonated compound is shown in Figure 30.

A more direct route to functionalized UMOFs is to use a phosphonic acid that is bound to the desired functional group. An example of this is the early work by Odobel et al., in which 2,2′-bipyridyl-5,5′-bis(phosphonic acid) was used as a pillar to form porous materials based on the α- and γ-zirconium phosphate structures.[81] The α-type compound was synthesized hydrothermally in a mixture of HF and DMSO. Phosphorous acid was used as a spacer ligand, resulting in a material with a surface area of 330 m^2/g and a large range of pore sizes. The other compound was synthesized by a topotactic exchange reaction of phosphate groups with 2,2′-bipyridyl-5,5′-bis(phosphonic acid) between the layers of γ-zirconium phosphate. This material had a surface area of 350 m^2/g and the pores were more uniform than in the α-phase,

dx.doi.org/10.1021/cr2002257 |Chem. Rev. 2012, 112, 1034–1054

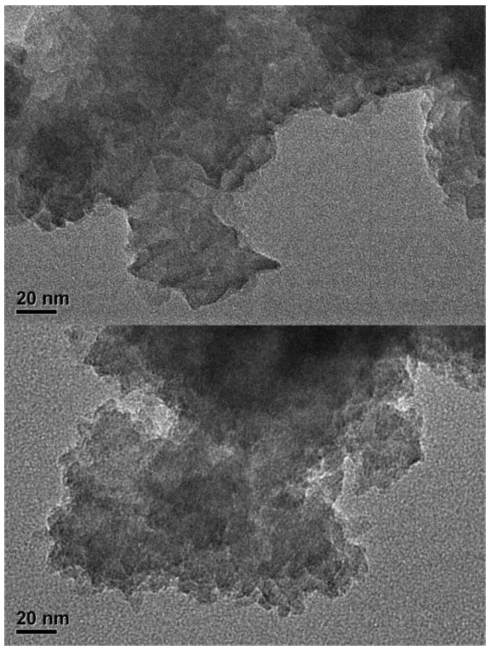

Figure 33. TEM images of **Sn1** (top) and **Sn6** (bottom).

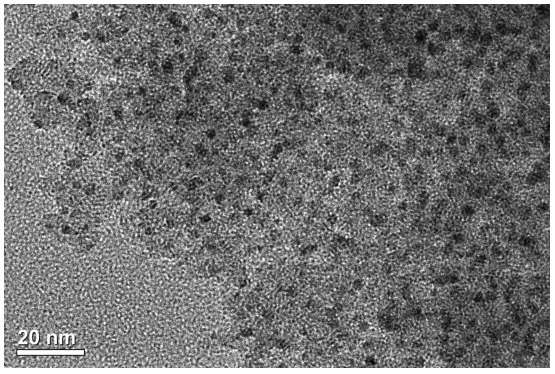

Figure 34. Pd nanoparticles supported on **Zr6**.

Table 7. Empirical Formulas Derived from the Elemental Analysis for the Zr Hybrids

sample	ratio	formula
1P-1	1:1	$Zr(C_6H_4P_2O_6)_{0.885}(HPO_4)_{0.229}\cdot 2.2H_2O$
1P-2	1:2	$Zr(C_6H_4P_2O_6)_{0.60}(HPO_4)_{0.80}\cdot 2.25H_2O$
1P-3	1:4	$Zr(C_6H_4P_2O_6)_{0.33}(HPO_4)_{1.34}\cdot 2.3H_2O$
1P-4	1:6	$Zr(C_6H_4P_2O_6)_{0.21}(HPO_4)_{1.58}\cdot 2.6H_2O$
1P-5	1:8	$Zr(C_6H_4P_2O_6)_{0.16}(HPO_4)_{1.69}\cdot 3.1H_2O$
2P-1	1:1	$Zr(C_{12}H_8P_2O_6)_{0.64}(HPO_4)_{0.71}\cdot 2H_2O$
2P-2	1:2	$Zr(C_{12}H_8P_2O_6)_{0.53}(HPO_4)_{0.94}\cdot 0.28H_2O$
2P-3	1:4	$Zr(C_{12}H_8P_2O_6)_{0.32}(HPO_4)_{1.36}\cdot 2.5H_2O$
2P-4	1:6	$Zr(C_{12}H_8P_2O_6)_{0.24}(HPO_4)_{1.51}\cdot 2.5H_2O$
2P-5	1:8	$Zr(C_{12}H_8P_2O_6)_{0.14}(HPO_4)_{1.72}\cdot 2.5H_2O$

with a maximum in the size distribution at ~5 Å. The α-phase material was shown to take up Fe(II) and Cu(I) from aqueous solutions at an amount corresponding to 100% occupation of the bipyridyl sites.

Table 8. K_d Values for the Alkali and Alkaline Earth Metal Ions for the Monophenyl (1P) and Biphenyl (2P) Phosphonate Phosphates at pH 3

sample	Li	Na	K	Rb	Cs	Mg	Ca	Sr	Ba
1P-1	<1	<1	<1	38	65	27	22	208	154
1P-2	<1	2.4	11	140	277	44	27	140	72
1P-3	5.8	5	97	288	2090	188	457	595	292
1P-4	1.9	2.4	123	522	3350	320	589	613	420
1P-5	<1	<1	133	220	4500	187	361	461	285
2P-1	<1	<1	6.6	<1	9.1	<1	<1	<1	<1
2P-2	<1	<1	12.3	<1	20	<1	<1	<1	<1
2P-3	10.1	5.5	43.7	51	102	35.7	37	20.4	51.3
2P-4	0.8	5.9	50.9	10	212	126	123	97.8	219
2P-5	10.9	11.3	126	34.8	1561	207	377	258	687

Table 9. K_d Values for Some Lanthanide Ions for the Zr Hybrids

sample	La	Eu	Gd	Dy
1P-1	12 700	17 600	93 200	78 500
1P-2	4 940	23 200	36 400	35 400
1P-3	23 000	158 000	119 000	132 000
1P-4	17 400	63 600	54 100	46 300
1P-5	33 000	313 000	231 000	
2P-1	411	587	922	1 230
2P-2	666	2 870	3 940	3 110
2P-3	3 700	9 950	10 100	13 200
2P-4	3 200	7 810	6 430	15 700
2P-5	6 460	9 710	17 800	17 600

In our most recent work in this area, we have synthesized a series of porous Zr-based frameworks that contained the 2, 2′-bipyridyl moiety and utilized methylphosphonic acid as a spacer ligand.[82] The spacer-to-pillar ratio was varied systematically from 6:1 to 0:1, and it was observed that the surface area increases as more spacer ligand is incorporated into the material. The compositions of these materials and their surface areas are given in Table 5. The tetraethyl ester of the bipyridylbisphosphonate pillar ligand (bpyBPAE) was used in the hydrothermal reactions and found to readily hydrolyze in-situ.

As with the other nearly amorphous phosphonate UMOFs, the PXRD patterns are generally of poor quality but can still provide important information about the nature of these materials. Figure 31 shows the PXRD patterns of the series of Zr compounds. They all showed a broad peak at ~13.5 Å, which was assigned to the interlayer spacing. The two compounds with the highest ratios of spacer to linker also showed a peak at ~10 Å, indicating that $Zr(O_3PCH_3)_2$ was present as an impurity phase. Another feature of the PXRD pattern was the gradual broadening of the peaks as the amount of spacer group was increased, which indicated that the particle sizes were decreasing as more spacer groups were incorporated into the material. Indeed, TEM images of the materials, shown in Figure 32, revealed that the particle sizes increased from ~8 nm to almost 20 nm as the ratio of spacer to pillar was decreased from 2:1 to 0:1. The TEM images also show that the particles are stacks of layers, confirming the *d*-spacing determined by PXRD.

As a comparison, we synthesized the analogous series of Sn(IV)-based compounds (Table 6), which showed some remarkable

dx.doi.org/10.1021/cr2002257 |*Chem. Rev.* 2012, 112, 1034–1054

Table 10. N_2 Sorption Surface Area Data Determined from BET and Percent Microporosity by t-Plot

	Zr inorganic−organic hybrid materials		Sn inorganic−organic hybrid materials	
synthesis temperature (°C)	total surface area (m^2/g)	microporous (%)	total surface area (m^2/g)	microporous (%)
80	547.8	55.77		
105	453.3	56.25		
120	452.3	71.48	270.6	98.62
145	443.8	44.95	268.6	95.20
160	342.3	62.78	290.4	96.49
180	473.3	42.76	339.2	95.34
200			342.2	94.36

Table 11. Nd^{3+} K_d Values Reported in mL/g

synthesis temp (°C)	Zr-hybrids	Sn-hybrids
80	82 472	
105	91 543	
120	74 971	32 428
145	77 125	59 852
160	77 744	35 351
180		40 870

Table 12. K_d Values Reported in mL/g

sample	Nd^{3+}	Sm^{3+}	Ho^{3+}	Yb^{3+}
H−Zr-hybrid	29 030	80 463	112 020	89 769
Na−Zr-hybrid	1 942 619	1 315 828	454 729	452 270
H−Sn-hybrid	337 525	317 477	322 933	159 301
Na−Sn-hybrid	480 067	296 704	216 026	216 383

differences from the Zr-based ones. Even at spacer-to-pillar ratios of 6:1, only one phase was obtained. Although the PXRD patterns looked practically identical, TEM (Figure 33) showed that the Sn compounds were highly disordered, and no stacks of layers were observed. Despite this apparently drastic difference, the Sn and Zr compounds had similar surface areas and thermal stabilities.

Both the Zr- and Sn-based materials were shown to chelate $Pd(O_2CCH_3)_2$ in the bipyridyl sites. In contrast with the results obtained by Odobel et al., only a fraction of the bipyridyl sites were occupied. This is in part due to the fact we used methylphosphonate as a spacer whereas Odobel and co-workers used the smaller phosphite spacer, which may allow less restricted diffusion of the metal ions through the pores.

Further functionalization of these UMOFs was achieved by reducing the Pd^{II} to form Pd^0 nanoparticles supported within the pore structure. Figure 34 shows the Pd nanoparticles supported on **Zr6**. It is interesting that these particles do not show any signs of agglomeration at temperatures up to 450 °C, even without the use of surfactants or stabilizers. We hypothesized that the spongelike pore structure may be limiting the mobility of the nanoparticles, thereby preventing agglomeration.

Another area of research that our group has been involved with for many years is the use of inorganic ion-exchange materials for

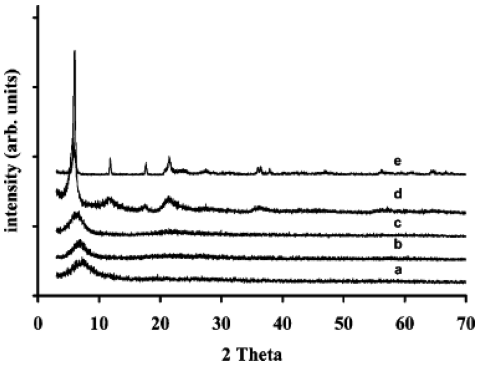

Figure 35. Powder XRD patterns of $Sn(O_3PC_6H_5)_2$. Samples were prepared by (a) room-temperature precipitation, (b) reflux for 1 h, (c) reflux for 12 h, (d) hydrothermal treatment at 140 °C for 3 days, and (e) hydrothermal treatment at 220 °C for 30 days.

the remediation of nuclear waste.[83] Now we are involved in considerations of problems associated with recovery of useful fuel from spent nuclear reactor fuel rods. The stability of Zr phosphates and phosphonates in acid solutions and their resistance to ionizing radiation makes them ideal candidates for ion-exchange materials used under these extreme conditions.

During the fission reactions in a nuclear pile, lower molecular weight elements are produced, largely Cs, Sr, and lanthanides. In addition, some of the uranium fuel is converted to Pu, Np, Am, and Cm isotopes. In recovering the valuable fuel, which consists of U, Pu, Np, and Am, it is necessary to remove the Cs, Sr, and lanthanides. In addition, Cm must be separated from Am because it is not desirable as part of the recovered fuel. Thus, based upon our earlier work we have set for ourselves the task of determining whether the Zr or Sn(IV) phosphonate UMOFs could possibly affect the separations required.

We chose to work with Zr and Sn(IV) BPBP with phosphate spacer groups to provide the functionality, an exchangeable proton. Our first task was to optimize the ratios of phosphoric acid to phosphonic acid.[84] The mixtures were heated at 80 °C for one day, resulting in highly amorphous solids. The *d*-spacings are somewhat larger than the more crystalline samples mentioned earlier, and the reflections are much broader. Table 7 lists the composition of the prepared samples. The ion-exchange distribution coefficients for the alkali metal and alkaline earth cations were determined in the usual way according to eq 1.

$$K_d = \frac{C_o - C_e}{C_e}\left(\frac{V}{M}\right) \quad (1)$$

where C_o is the initial ion concentration and C_e is the equilibrium concentration, V is the volume of solution, and M is the mass of the ion exchanger. The units are mL/g. The K_d then represents the total uptake of the cation divided by the amount of ion left in solution, standardized by the volume-to-mass ratio. The results listed in Table 8 for alkali and alkaline earth cations are very low except for Cs^+ ion in some samples. In contrast, the values for lanthanides are quite high and better for the monophenyl exchangers than the biphenyl, as shown in Table 9. This result was unexpected as normally one would expect that, if charge were the only factor, the K_d values for the alkaline earth cations would be intermediate between the monovalent and trivalent cations. We have now applied these interesting properties to a problem in the nuclear fuel cycle.

dx.doi.org/10.1021/cr2002257 |*Chem. Rev.* 2012, 112, 1034–1054

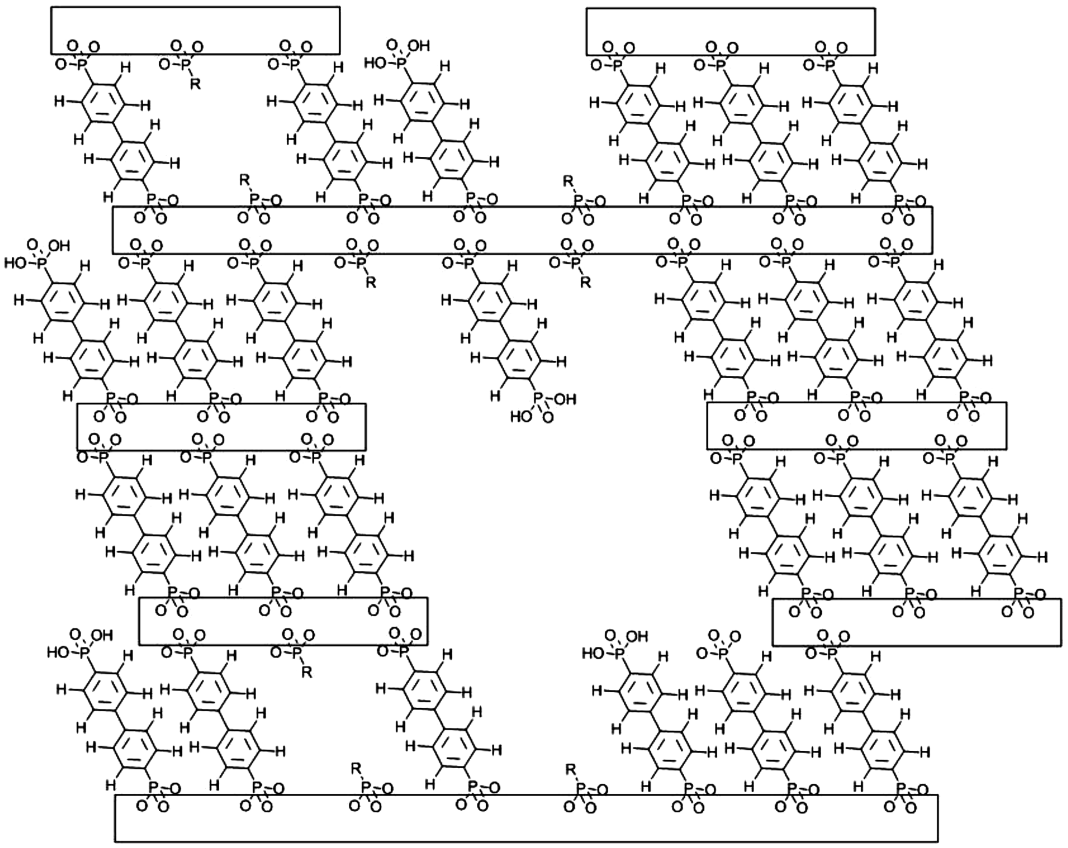

Figure 36. Schematic drawing of how micropores may be formed in the M(IV) phosphonate UMOFs. The horizontal rectangles represent the inorganic layers (M = Zr or Sn) that are cross-linked by the organic moieties. R stands for H, OH, or CH_3, and the surfaces are capped by M because an excess of metal is used in the syntheses.

In further exploration of this system, we have synthesized two types of Zr and Sn(IV) monophenylbisphosphonate UMOFs: those in which the spacer group is derived from phosphoric acid and those prepared with Na_3PO_4 to provide a Na^+ exchanger. A composition of $M(O_3PC_6H_4PO_3)_{0.5}(O_3POH)\cdot nH_2O$ was chosen, and the preparation temperature was varied to determine its effect on the surface area.[85]

The effect of temperature of preparation on the surface areas and pore sizes for groups of Zr and Sn(IV) bisphosphonate−phosphates is shown in Table 10. For the Zr derivatives, the surface areas do not vary in any systematic way, nor does the percent of microporosity. In the case of the Sn compounds, the surface area increases with increase in temperature of preparation and the microporosity is uniformly high. The K_d values of these preparations for Nd at pH = 3 are given in Table 11. There is some variation in the values, but they are uniformly high and higher for the Zr samples than those for Sn. The samples made with substitution of Na_3PO_4 for phosphoric acid showed a significant increase in K_d values in the pH = 3−3.3 region. However, we were not expecting the actual results collected. On the basis of this temperature study and one in which we optimized the time of reaction, we prepared four hybrids at 140 °C for four days. Two of the samples were prepared using Na_3PO_4 in place of phosphoric acid. The K_d values for selected lanthanides at pH = 3 are presented in Table 12. These results are exceptionally good as extremely high K_d values were recorded utilizing 10^{-4} M Ln (10 mL) and 20 mg of hybrid exchanger.

Preliminary studies with actinides indicate that NpO_2^+ and PuO_2^{2+} are not taken up by the hybrids at pH ≈ 2, similarly to the alkali and alkaline earth cations. However, as tri- or tetravalent cations they are selectively taken up at pH ≈ 2. This would appear to be a basis for group separations based upon oxidation states and pH manipulation. We are pursuing these lines of investigation.[85]

3.5. Some Remarks on the Structure of Phosphonate UMOFs

The key to understanding the properties of any material lies in understanding its structure. UMOFs present a unique opportunity to establish structure−property relationships for a class of materials that have no regular structure. Instead of a well-defined set of atomic coordinates from a single crystal structure solution, we must form a general model of the structure which takes into account defects, surfaces, and irregularity if we are to draw conclusions about the structure−property relationships of these materials. That model and its variants need to explain the following observations: (1) the compounds are nanosized particles with no long-range order; (2) the pore sizes often exceed those predicted on the basis of the interlayer spaces; (3) choice of solvent may change the pore structure as shown by the change in N_2 sorption isotherms; (4) the use of templates may change the pore structure; (5) the insertion of phenyl rings as spacers in biphenyl pillared UMOFs does not increase the interlayer spacing; (6) the stoichiometry may deviate from a 2:1 phosphorus to metal ratio due to hydrolysis (P/M < 2:1) or large external surface (P/M > 2:1);[77] and (7) the compounds are aggregates of nanoparticles and addition of a second ligand reduces the particle size.

dx.doi.org/10.1021/cr2002257 |*Chem. Rev.* 2012, 112, 1034–1054

There is no doubt that these M(IV) phosphonates have special growth patterns that prevent crystallization. In the case of non-cross-linked phenyl phosphonates, progression toward crystallinity is very slow as evidenced for $Sn(O_3PC_6H_5)_2$ in Figure 35.[75] The same is true for the zirconium analogue. After heating at 200 °C for 30 days, a powder pattern with ~40−50 usable reflections led to a structure solution.[67] Similarly, extended hydrothermal treatment of Sn(IV) methylphosphonate allowed for structure solution of this compound.[77]

In contrast to the materials that are not crosslinked, heating only slightly improves the X-ray patterns of the bisphosphonates sufficiently to allow a structure solution. This is apparently due to the great insolubility of these preparations. Even with HF added as a solubilizing agent, the results are similar. Crystalline phosphonate MOFs have been prepared as detailed in the beginning of this paper, but they utilize lower-valence cations. UMOFs must have a growth pattern that prevents the formation of long-range order. As shown in Figure 35, the broadness of the peaks indicates that very small particles form during the early stages of the synthesis. In the initial stages the phosphonic acid needs to contact three M(IV) ions to have bonding of the type that exists in $Zr(O_3PC_6H_5)_2$ or in α-zirconium phosphate, $Zr(O_3POH)_2 \cdot H_2O$.[68] Once a ligand is bonded in this way, a layer begins to grow, essentially immobilizing the ligand. The other end of the ligand then needs to wait until three M(IV) ions are in position to bond. This process is dynamic and complicated by the extreme lack of solubility, which inhibits annealing and ripening mechanisms. One would expect then that the two layers would grow at separate rates. This uneven growth would be expected to leave gaps in the layer, and in some cases the other end of the ligand might not bond at all. A schematic drawing of such a structure is shown in Figure 36. Because the process is random, the exact internal structure may depend upon a host of conditions such as solvent, template, temperature, ratio of reactants, or relative solubility of the two ligands.

The proposed model explains how the pores can be larger than the interlayer distance and why a spacer molecule such as phenyl phosphonic acid does not increase the interlayer distance. However, one might expect a different pore structure from use of methylphosphonic acid. More work needs to be done to fully characterize the pores within these materials and to learn to tune both their size and chemical nature for various applications.

4. SUMMARY AND FUTURE OUTLOOK

The field of MOF chemistry is no longer in its infancy, yet it is far from mature. There are many possible applications and extensions of these materials that are yet to be discovered, and they may prove useful in countless fields and technologies. Both crystalline and UMOF-type phosphonate MOFs will play an important role in the advancement of this field as counterparts to traditional carboxylate-based materials. PXRD will continue to be an invaluable tool in characterizing phosphonate-based MOFs. Other methods used in the characterization of poorly ordered materials, such as pair distribution function (PDF) analysis, EXAFS/XANES, and positron annihilation lifetime spectroscopy, should also be used to study the nature of the defects within their structures. It should be noted that reports of mixed carboxylate−phosphonate materials are becoming quite common, and it may be that these types of materials will bridge the gap between the world of crystalline, ordered MOFs and that of robust but amorphous UMOFs.

High-throughput synthetic techniques allow for rapid and automated screening of solvents and conditions to obtain new materials. However, the future of the field may not depend on our ability to generate more and more new compounds but instead on our ability to understand structure−property relationships and find novel applications for the compounds we already have.

AUTHOR INFORMATION

Corresponding Author

*E-mail: Clearfield@mail.chem.tamu.edu.

BIOGRAPHIES

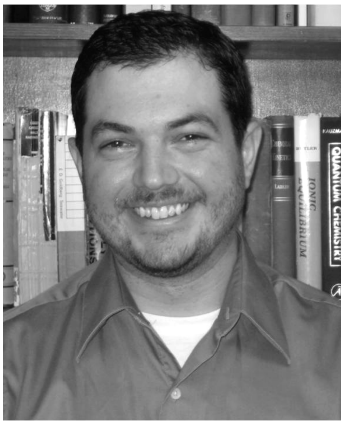

Kevin Gagnon was born in 1986 in Southborough, Massachusetts. He earned a B.S. degree in Chemistry from Worcester Polytechnic Institute (WPI) in 2008. During his time there he maintained an internship working for American Superconductor Corporation in Devens, MA, and also worked as a student researcher under the supervision of Dr. Venkat Thalladi at WPI. In 2008 he joined the research group of Dr. Abraham Clearfield at Texas A&M University, where he is pursuing his Ph. D. and currently studies ionothermal synthesis of phosphonate materials.

Dr. Houston Perry was born in 1982 near Fort Worth, Texas. He earned his B.S. degree in Chemistry from Texas A&M University in 2005. His undergraduate research was focused on the synthesis and characterization of selective ion exchangers for use in nuclear waste remediation. He graduated with his Ph.D. in chemistry from Texas A&M University in 2011, where he worked with Dr. Clearfield developing techniques to obtain functional phosphonate-based materials.

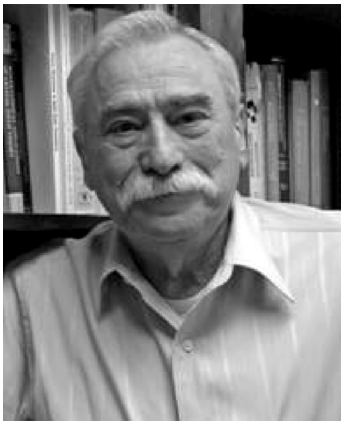

Dr. Clearfield received his B.A. and M.A. from Temple University in Philadelphia and his Ph.D. at Rutgers University in 1954. His Ph.D. training was in inorganic chemistry and crystallography. He worked in industry before he joined the faculty of Ohio University in 1963. In 1976 he joined the faculty at Texas A&M University, where he is currently a distinguished professor. During his academic tenure he has mentored over 30 Ph.D. students and 45 postdocs, in addition to numerous undergraduates. He has extensively studied phosphates, phosphonates, and other layered materials, having published nearly 600 papers. His early work on the syntheses and crystal structures of zirconium phosphates laid the foundation for a worldwide research effort that continues to this day.

ACKNOWLEDGMENT

The authors thankfully acknowledge the National Science Foundation (Grants DMR-0652166, HRD-0832993, and DGE-0750732), the Department of Energy (Grant DE-FG02-03ER15420), Savannah River National Laboratory (Grant AC-70059-0), and the Robert A. Welch Foundation (Grant A0673) for financial support.

LIST OF ABBREVIATIONS

BPDP	biphenyldiphosphonate
BTPH6	benzenetris(phosphonic acid)
4-cppH3	4-carboxyphenylphosphonic acid
dabco	1,4-diazabicyclo[2.2.2]octane
MOF	metal−organic framework
PDF	pair distribution function
PPPA	4-(4′-phosphonophenoxy)phenylphosphonic acid
PXRD	powder X-ray diffraction
SDS	sodium dodecyl sulfate
UMOF	unconventional metal−organic framework

REFERENCES

(1) Barthelet, K.; Marrot, J.; Riou, D.; Férey, G. *Angew. Chem., Int. Ed.* **2002**, *41* (2), 281.
(2) Eddaoudi, M.; Kim, J.; Rosi, N.; Vodak, D.; Wachter, J.; O'Keeffe, M.; Yaghi, O. M. *Science* **2002**, *295* (5554), 469.
(3) Millange, F.; Serre, C.; Ferey, G. *Chem. Commun.* **2002**, No. 8, 822.
(4) Yaghi, O. M.; O'Keeffe, M.; Ockwig, N. W.; Chae, H. K.; Eddaoudi, M.; Kim, J. *Nature* **2003**, *423* (6941), 705.
(5) Rowsell, J. L. C.; Millward, A. R.; Park, K. S.; Yaghi, O. M. *J. Am. Chem. Soc.* **2004**, *126* (18), 5666.
(6) Férey, G.; Mellot-Draznieks, C.; Serre, C.; Millange, F.; Dutour, J.; Surblé, S.; Margiolaki, I. *Science* **2005**, *309* (5743), 2040.
(7) Colombo, V.; Galli, S.; Choi, H. J.; Han, G. D.; Maspero, A.; Palmisano, G.; Masciocchi, N.; Long, J. R. *Chem. Sci.* **2011**, *2* (7), 1311.
(8) Clearfield, A.; Demadis, K. *Metal Phosphonate Chemistry: From Synthesis to Applications*; RSC: Cambridge, U.K., 2011; pp 457.
(9) Dines, M. B.; Cooksey, R. E.; Griffith, P. C.; Lane, R. H. *Inorg. Chem.* **1983**, *22* (6), 1003.
(10) Clearfield, A. *Dalton Trans.* **2008**, No. 44, 6089.
(11) Le Bideau, J.; Payen, C.; Palvadeau, P.; Bujoli, B. *Inorg. Chem.* **1994**, *33* (22), 4885.
(12) Maeda, K.; Kiyozumi, Y.; Mizukami, F. *Angew. Chem., Int. Ed. Engl.* **1994**, *33* (22), 2335.
(13) Maeda, K.; Akimoto, J.; Kiyozumi, Y.; Mizukami, F. *Angew. Chem., Int. Ed. Engl.* **1995**, *34* (11), 1199.
(14) Maeda, K.; Akimoto, J.; Kiyozumi, Y.; Mizukami, F. *J. Chem. Soc., Chem. Commun.* **1995**, No. 10, 1033.
(15) Herdes, C.; Valente, A.; Lin, Z.; Rocha, J.; Coutinho, J. A. P.; Medina, F.; Vega, L. F. *Langmuir* **2007**, *23* (13), 7299.
(16) Shimizu, G. K. H.; Vaidhyanathan, R.; Taylor, J. M. *Chem. Soc. Rev.* **2009**, *38* (5), 1430.
(17) Maeda, K. *Microporous Mesoporous Mater.* **2004**, *73* (1−2), 47.
(18) Miller, S. R.; Lear, E.; Gonzalez, J.; Slawin, A. M. Z.; Wright, P. A.; Guillou, N.; Ferey, G. *Dalton Trans.* **2005**, No. 20, 3319.
(19) Zhang, Y.-Y.; Qi, Y.; Zhang, Y.; Liu, Z.-Y.; Zhao, Y.-F.; Liu, Z.-M. *Mater. Res. Bull.* **2007**, *42* (8), 1531.
(20) Lohse, D. L.; Sevov, S. C. *Angew. Chem., Int. Ed. Engl.* **1997**, *36* (15), 1619.
(21) Gao, Q.; Guillou, N.; Nogues, M.; Cheetham, A. K.; Férey, G. *Chem. Mater.* **1999**, *11* (10), 2937.
(22) Nelson, A.-G. D.; Albrecht-Schmitt, T. E. *C. R. Chim.* **2010**, *13* (6−7), 755.
(23) Knope, K. E.; Cahill, C. L. *Dalton Trans.* **2010**, *39* (35), 8319.
(24) Merrill, C. A.; Cheetham, A. K. *Inorg. Chem.* **2005**, *44* (15), 5273.
(25) Merrill, C. A.; Cheetham, A. K. *Inorg. Chem.* **2007**, *46* (1), 278.
(26) Yuan, Z.; Clegg, W.; Attfield, M. P. *J. Solid State Chem.* **2009**, *182* (11), 3049.
(27) Poojary, D. M.; Zhang, B.; Clearfield, A. *J. Am. Chem. Soc.* **1997**, *119* (51), 12550.
(28) Poojary, D. M.; Zhang, B.; Clearfield, A. *Chem. Mater.* **1999**, *11* (2), 421.
(29) Arnold, D. I.; Ouyang, X.; Clearfield, A. *Chem. Mater.* **2002**, *14* (5), 2020.
(30) Clearfield, A.; Wang, Z. *J. Chem. Soc., Dalton Trans.* **2002**, No. 15, 2937.
(31) Finn, R. C.; Zubieta, J.; Haushalter, R. C. *Crystal Chemistry of Organically Templated Vanadium Phosphates and Organophosphonates*; John Wiley & Sons, Inc.: New York, 2003; p 421.
(32) Fu, R.-B.; Wu, X.-T.; Hu, S.-M.; Zhang, J.-J.; Fu, Z.-Y.; Du, W.-X. *Polyhedron* **2003**, *22* (19), 2739.
(33) Fu, R.; Huang, X.; Hu, S.; Xiang, S.; Wu, X. *Inorg. Chem.* **2006**, *45* (14), 5254.
(34) Ouellette, W.; Yu, M. H.; O'Connor, C. J.; Zubieta, J. *Inorg. Chem.* **2006**, *45* (8), 3224.
(35) Attfield, M. P.; Yuan, Z.; Harvey, H. G.; Clegg, W. *Inorg. Chem.* **2010**, *49* (6), 2656.
(36) Soghomonian, V.; Chen, Q.; Haushalter, R. C.; O'Connor, C. J.; Tao, C.; Zubieta, J. *Inorg. Chem.* **1995**, *34* (13), 3509.
(37) LaDuca, R.; Rose, D.; DeBord, J. R. D.; Haushalter, R. C.; O'Connor, C. J.; Zubieta, J. *J. Solid State Chem.* **1996**, *123* (2), 408.
(38) Groves, J. A.; Miller, S. R.; Warrender, S. J.; Mellot-Draznieks, C.; Lightfoot, P.; Wright, P. A. *Chem. Commun.* **2006**, No. 31, 3305.
(39) Serre, C.; Groves, J. A.; Lightfoot, P.; Slawin, A. M. Z.; Wright, P. A.; Stock, N.; Bein, T.; Haouas, M.; Taulelle, F.; Férey, G. *Chem. Mater.* **2006**, *18* (6), 1451.
(40) Miller, S. R.; Pearce, G. M.; Wright, P. A.; Bonino, F.; Chavan, S.; Bordiga, S.; Margiolaki, I.; Guillou, N.; Férey, G.; Bourrelly, S.; Llewellyn, P. L. *J. Am. Chem. Soc.* **2008**, *130* (47), 15967.

(41) Groves, J. A.; Stephens, N. F.; Wright, P. A.; Lightfoot, P. *Solid State Sci.* **2006**, *8* (3−4), 397.
(42) Wharmby, M. T.; Miller, S. R.; Groves, J. A.; Margiolaki, I.; Ashbrook, S. E.; Wright, P. A. *Dalton Trans.* **2010**, *39* (28), 6389.
(43) Mowat, J. P. S.; Groves, J. A.; Wharmby, M. T.; Miller, S. R.; Li, Y.; Lightfoot, P.; Wright, P. A. *J. Solid State Chem.* **2009**, *182* (10), 2769.
(44) Du, Z.-Y.; Xu, H.-B.; Mao, J.-G. *Inorg. Chem.* **2006**, *45* (24), 9780.
(45) Wharmby, M. T.; Mowat, J. P. S.; Thompson, S. P.; Wright, P. A. *J. Am. Chem. Soc.* **2011**, *133* (5), 1266.
(46) Costantino, F.; Gentili, P. L.; Audebrand, N. *Inorg. Chem. Commun.* **2009**, *12* (5), 406.
(47) Taddei, M.; Costantino, F.; Vivani, R. *Inorg. Chem.* **2010**, *49* (20), 9664.
(48) Poojary, D. M.; Grohol, D.; Clearfield, A. *Angew. Chem., Int. Ed. Engl.* **1995**, *34* (13−14), 1508.
(49) Cao, G.; Lee, H.; Lynch, V. M.; Mallouk, T. E. *Solid State Ionics* **1988**, *26* (2), 63.
(50) Grohol, D.; Clearfield, A. *J. Am. Chem. Soc.* **1997**, *119* (20), 4662.
(51) Poojary, D. M.; Cabeza, A.; Aranda, M. A. G.; Bruque, S.; Clearfield, A. *Inorg. Chem.* **1996**, *35* (6), 1468.
(52) Aranda, M. A. G.; Cabeza, A.; Bruque, S.; Poojary, D. M.; Clearfield, A. *Inorg. Chem.* **1998**, *37* (8), 1827.
(53) Li, J.-T.; Cao, D.-K.; Liu, B.; Li, Y.-Z.; Zheng, L.-M. *Cryst. Growth Des.* **2008**, *8* (8), 2950.
(54) Taylor, J. M.; Mahmoudkhani, A. H.; Shimizu, G. K. H. *Angew. Chem., Int. Ed.* **2007**, *46* (5), 795.
(55) Vaidhyanathan, R.; Liang, J.; Iremonger, S. S.; Shimizu, G. K. H. *Supramol. Chem.* **2011**, *23* (3), 278.
(56) Chen, Z.; Zhou, Y.; Weng, L.; Yuan, C.; Zhao, D. *Chem.—Asian J.* **2007**, *2* (12), 1549.
(57) Chen, Z.; Zhou, Y.; Weng, L.; Zhao, D. *Cryst. Growth Des.* **2008**, *8* (11), 4045.
(58) Taylor, J. M.; Mah, R. K.; Moudrakovski, I. L.; Ratcliffe, C. I.; Vaidhyanathan, R.; Shimizu, G. K. H. *J. Am. Chem. Soc.* **2010**, *132* (40), 14055.
(59) Vaidhyanathan, R.; Mahmoudkhani, A. H.; Shimizu, G. K. H. *Can. J. Chem.* **2009**, *87* (1), 247.
(60) Wang, Z.; Heising, J. M.; Clearfield, A. *J. Am. Chem. Soc.* **2003**, *125* (34), 10375.
(61) Brunet, E.; Cerro, C.; Juanes, O.; Rodríguez-Ubis, J. C.; Clearfield, A. *J. Mater. Sci.* **2008**, *43* (3), 1155.
(62) Cabeza, A.; Aranda, M. A. G.; Bruque, S.; Poojary, D. M.; Clearfield, A.; Sanz, J. *Inorg. Chem.* **1998**, *37* (17), 4168.
(63) Gómez-Alcántara, M. d. M.; Cabeza, A.; Moreno-Real, L.; Aranda, M. A. G.; Clearfield, A. *Microporous Mesoporous Mater.* **2006**, *88* (1−3), 293.
(64) Sing, K. S. W.; Everett, D. H.; Haul, R. A. W.; Moscou, L.; Pierotti, R. A.; Rouquerol, J.; Siemieniewska, T. *Pure Appl. Chem.* **1985**, *57* (4), 603.
(65) Clearfield, A.; Wang, Z.; Bellinghausen, P. *J. Solid State Chem.* **2002**, *167* (2), 376.
(66) Alberti, G.; Costantino, U.; Marmottini, F.; Vivani, R.; Zappelli, P. *Angew. Chem., Int. Ed. Engl.* **1993**, *32* (9), 1357.
(67) Poojary, M. D.; Hu, H.-L.; Campbell, F. L., III; Clearfield, A. *Acta Crystallogr., Sect. B: Struct. Sci.* **1993**, *49* (6), 996.
(68) Clearfield, A.; Smith, G. D. *Inorg. Chem.* **1969**, *8* (3), 431.
(69) Troup, J. M.; Clearfield, A. *Inorg. Chem.* **1977**, *16* (12), 3311.
(70) Clearfield, A. Metal Phosphonate Chemistry. In *Prog. Inorg. Chem.*; Karlin, K. D., Ed.; John Wiley & Sons, Inc.: New York, 1998.
(71) Mal, N. K.; Fujiwara, M.; Yamada, Y.; Kuraoka, K.; Matsukata, M. *J. Ceram. Soc. Jpn.* **2003**, *111* (1292), 219.
(72) Mal, N. K.; Fujiwara, M.; Yamada, Y.; Matsukata, M. *Chem. Lett.* **2003**, *32* (3), 292.
(73) Mal, N. K.; Fujiwara, M.; Matsukata, M. *Chem. Commun.* **2005**, No. 41, 5199.
(74) Subbiah, A.; Pyle, D.; Rowland, A.; Huang, J.; Narayanan, R. A.; Thiyagarajan, P.; Zoń, J.; Clearfield, A. *J. Am. Chem. Soc.* **2005**, *127* (31), 10826.
(75) Huang, J.; Subbiah, A.; Pyle, D.; Rowland, A.; Smith, B.; Clearfield, A. *Chem. Mater.* **2006**, *18* (22), 5213.
(76) Kirumakki, S.; Samarajeewa, S.; Harwell, R.; Mukherjee, A.; Herber, R. H.; Clearfield, A. *Chem. Commun.* **2008**, No. 43, 5556.
(77) Kirumakki, S.; Huang, J.; Subbiah, A.; Yao, J.; Rowland, A.; Smith, B.; Mukherjee, A.; Samarajeewa, S.; Clearfield, A. *J. Mater. Chem.* **2009**, *19* (17), 2593.
(78) Gomez-Alcantara, M. d. M.; Cabeza, A.; Olivera-Pastor, P.; Fernandez-Moreno, F.; Sobrados, I.; Sanz, J.; Morris, R. E.; Clearfield, A.; Aranda, M. A. G. *Dalton Trans.* **2007**, No. 23, 2394.
(79) Yang, C.-Y.; Clearfield, A. *React. Polym., Ion Exchangers, Sorbents* **1987**, *5* (1), 13.
(80) Stein, E. W.; Clearfield, A.; Subramanian, M. A. *Solid State Ionics* **1996**, *83* (1−2), 113.
(81) Odobel, F.; Bujoli, B.; Massiot, D. *Chem. Mater.* **2001**, *13* (1), 163.
(82) Perry, H. P.; Law, J.; Zon, J.; Clearfield, A. *Microporous Mesoporous Mater.* **2011**, *149* (1), 172.
(83) Celestian, A. J.; Parise, J. B.; Clearfield, A. Crystal Growth and Ion Exchange in Titanium Silicates. In *Springer Handbook of Crystal Growth*; Dhanaraj, G., Byrappa, K., Prasad, V., Dudley, M., Eds.; Springer: Berlin/Heidelberg, 2010; p 1637.
(84) Cahill, R.; Shpeizer, B.; Peng, G. Z.; Bortun, L.; Clearfield, A. Separations of f Elements; Proceedings of an American Chemical Society Symposium on f Elements Separations, San Diego, Mar. 13−17, *1994*; p 165.
(85) Burns, J.; Clearfield, A.; Borkowski, M.; Reed, D. *Radiochim. Acta* **2012**, in press.